NASA
Technical
Paper
3154

September 1991

Application and Flight Test of Linearizing Transformations Using Measurement Feedback to the Nonlinear Control Problem

Robert F. Antoniewicz,
Eugene L. Duke,
and P. K. A. Menon

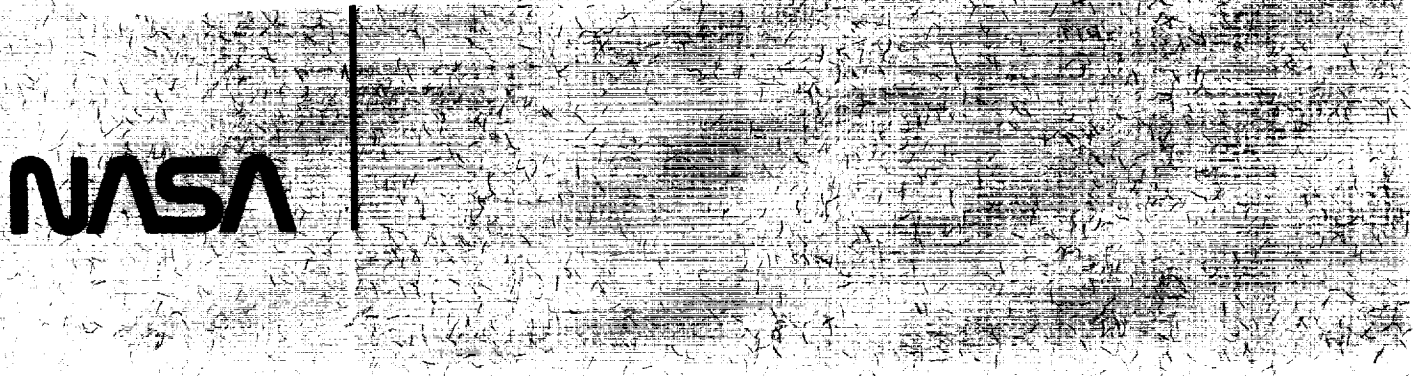

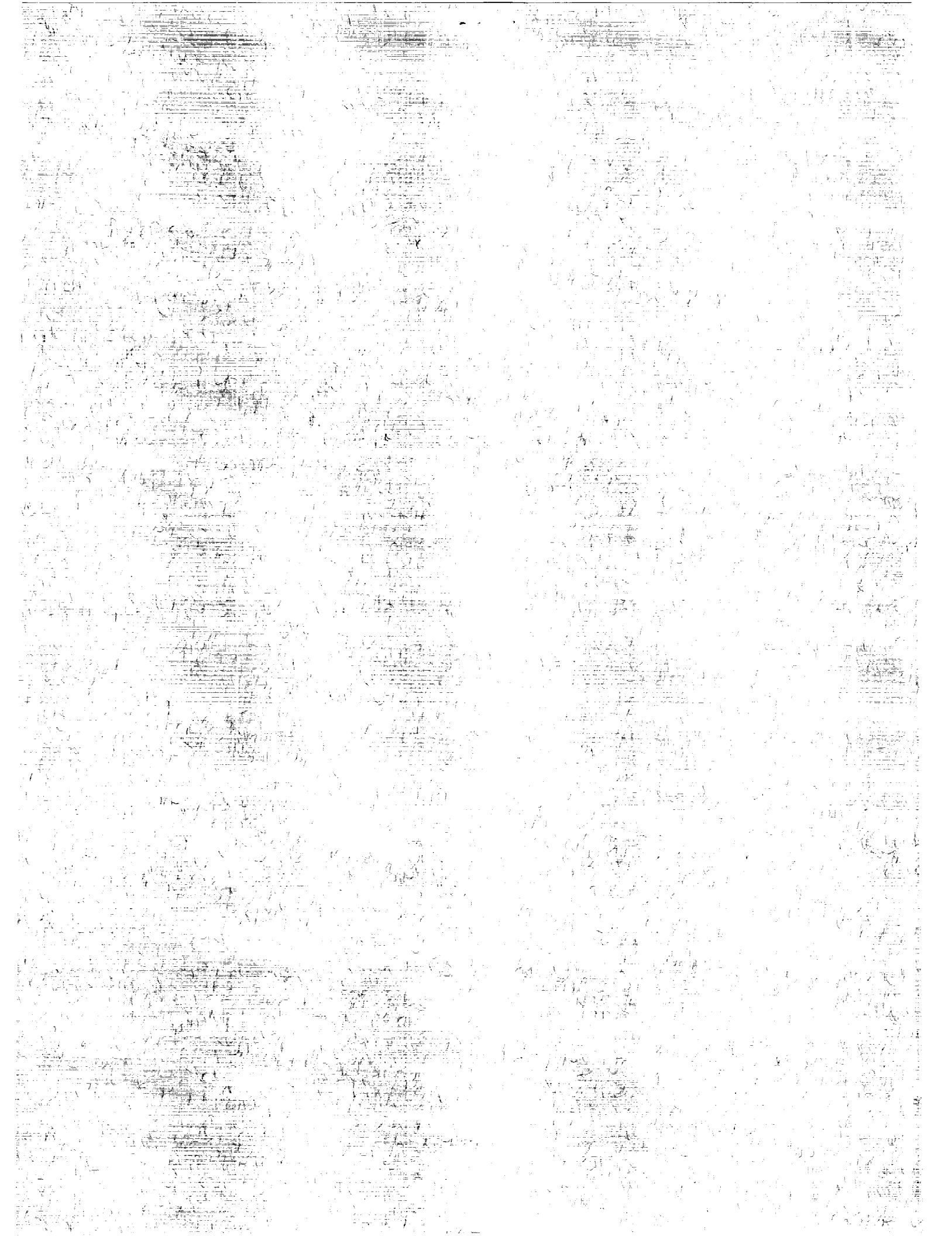

NASA Technical Paper 3154

1991

Application and Flight Test of Linearizing Transformations Using Measurement Feedback to the Nonlinear Control Problem

Robert F. Antoniewicz
and Eugene L. Duke
Dryden Flight Research Facility
Edwards, California

P. K. A. Menon
Georgia Institute of Technology
Atlanta, Georgia

National Aeronautics and Space Administration
Office of Management
Scientific and Technical Information Program

CONTENTS

SUMMARY

The design of nonlinear controllers has relied on the use of detailed aerodynamic and engine models that must be associated with the control law in the flight system implementation. Many of these controllers have been applied to vehicle flightpath control problems and have attempted to combine both inner- and outer-loop control functions in a single controller. In this paper, a new approach to the nonlinear trajectory control problem is presented. This approach uses linearizing transformations with measurement feedback to eliminate the need for detailed aircraft models in outer-loop control applications. By applying this approach and separating the inner-loop and outer-loop functions two things are achieved: (1) the need for incorporating detailed aerodynamic models in the controller is obviated and (2) the controller is more easily incorporated into existing aircraft flight-control systems. This paper also discusses an implementation of the controller described here. This controller is tested on a six degree-of-freedom F-15 simulation and in flight on an F-15 aircraft. Simulation data are presented which validates this approach over a large portion of the F-15 flight envelope. Proof of this concept is provided by flight-test data that closely matches simulation results. Flight-test data are also presented.

INTRODUCTION

The problem of aircraft trajectory control is generally thought of as an "outer-loop" problem, that is, the aircraft is assumed to have a stabilizing, "inner-loop" command augmentation system through which the pilot or automatic trajectory control system interacts with the vehicle control effectors (such as the elevators, ailerons, and rudder). In fact, for a great number of trajectory control problems, it is the pilot who provides this outer-loop control by translating a mental image of the trajectory into stick, pedal, and throttle commands using feedback information provided by the crew station instruments. Outer-loop control may also be provided by an autopilot that performs simple tasks like maintaining altitude and velocity or one that performs more complex tasks such as automatic landing.

Inner-loop control generally refers to control of the aircraft about its center of mass; outer-loop control refers to the control of the trajectory of the center of mass. The former is generally called "the control problem" while the latter is often referred to as "the guidance problem."

This distinction between inner-loop and outer-loop functions is important for two reasons: (1) the frequency response requirements of these functions are significantly different and (2) the output commands from the two types of controllers differ significantly.

The frequency response requirements for inner-loop control are generally on the order of 1 to 30 rad/sec, because of the dynamic characteristics of high performance aircraft. The frequency response requirements for outer-loop control are on the order of 0.1 to 3 rad/sec, because of the trajectory tracking requirements. The outputs from an inner-loop control system are essentially surface position commands; the outputs from an outer-loop controller are similar to stick, pedal, and throttle position commands. The two types of controllers are usually separate designs and distinct subsystems.

The fundamental objective of trajectory control research at the Dryden Flight Research Facility is to define a generic approach for designing control laws that will command an aircraft to fly precise flight-test maneuvers to obtain accurate, repeatable flight data. The intent is to use modern control theory design techniques to lay out a method of designing flight-test trajectory controllers for various aircraft at Dryden to improve data collection performance. The approach should also be applicable to other aircraft for the design of items such as autopilots and automatic navigation systems. Implicit in this objective is the requirement to develop control laws using different techniques for a candidate aircraft and subsequently to evaluate the performance and assess the limitations of these control laws. The candidate aircraft is the NASA F-15 highly integrated digital electronic control (HIDEC) aircraft [1].

Over the past several years, techniques such as eigenstructure assignment, linear optimal control, and others were applied in the attempt to find a design approach. However, the most promising technique involves the use of nonlinear inverse transformation theory. Inverse transformations relate the input of the linearized aircraft system to the required aircraft command augmentation system (CAS) nonlinear input. The application of this theory to flight-test trajectory control has been treated by Menon *et al* [2,3]. This application uses the equations of motion and inverse aerodynamic and engine models to provide inputs to the inner-loop controller of the aircraft. The methodology for the use of nonlinear inverse transformations and inverse models presented in this paper is based primarily on the work of Meyer and Cicolani [4,5], Meyer [6], and Meyer *et al* [7] whose approach is presented in some detail. The perceived limitations of the work by previous authors are discussed.

This paper presents the theory for and an application of an approach that provides a new solution to the flight-test trajectory control problem. The elegance of this solution is that the control laws are obtained from flat, nonrotating Earth, equations of motion with accelerometer outputs providing force data instead of an aerodynamic model. This makes the controller easy to apply to different aircraft since only a simple inverse engine model is required. The use of nonlinear inverse transformations presents a linear system to the designer for which simple proportional-integral, or proportional-integral-derivative control laws using a single set of gains need be designed.

A flight-test trajectory controller (FTTC) was designed using this new approach and was tested on a real-time, six-degree-of-freedom, full envelope, nonlinear simulation of an F-15 aircraft. Various maneuvers were simulated over a Mach number range of 0.60 to 1.20, over an altitude range of 10,000 ft to 40,000 ft. Simulation results justified flight test of the FTTC with the F-15 HIDEC aircraft. Flight test covered a subset of the maneuvers tested in the simulation. Both simulation and flight-test results are presented.

NOMENCLATURE

Acronyms

AWJSRA	augmentor wing jet short takeoff and landing research aircraft
CAS	command augmentation system
FTTC	flight-test trajectory control
FTTG	flight-test trajectory guidance
HIDEC	highly integrated digital electronic control
HiMAT	highly maneuverable aircraft technology
PLA	power lever angle, deg
RAV	remotely augmented vehicle
STO	short takeoff and landing
TAFCOS	total automatic flight-control system
VATO	vertical attitude takeoff and landing
WATR	Western Aeronautical Test Range

Symbols

A	angles; plant matrix
A_0	servo plant matrix
a	acoustic velocity, ft/sec

a_n	body axis normal accelerometer output, g
a_x	x-axis body accelerometer output, g
a_y	y-axis body accelerometer output, g
a_z	z-axis body accelerometer output, g
B	control matrix
B_0	servo control matrix
D	aircraft total drag, lb
$\mathbf{e}$	error signal vector
e	error signal
$\mathbf{f}$	aircraft nonlinear functions
$\mathbf{g}$	aircraft nonlinear control functions
g	gravitational acceleration, ft/sec^2
$\mathbf{h}$	aircraft measurement functions
h	altitude, ft
$\dot{h}$	altitude rate, ft/sec
$\ddot{h}$	vertical acceleration, ft/sec^2
$\mathbf{K}$	gain matrix
L	total aerodynamic lift, lb
M	Mach number
m	mass, slugs
PLA_{com}	commanded power lever angle, deg
p	body axis roll rate, deg/sec; power state
$\dot{p}$	power rate, ft/sec
p_{com}	commanded body axis roll rate, deg/sec
q	body axis pitch rate, deg/sec
q_{com}	commanded body axis pitch rate, deg/sec
r	body axis yaw rate, deg/sec; position state
r^*	reference trajectory
$\Re$	set of real numbers
$\mathbf{S}$	transformation from body-axis rotational rates to inertial angle rotational rates
$\mathbf{T}$	linearizing transformation
T	total thrust, lb
$\mathbf{u}$	nonlinear input vector
u	aircraft x-body axis velocity, ft/sec
$\dot{u}$	aircraft x-body axis kinematic acceleration, ft/sec^2
V	total velocity, ft/sec
$\dot{V}$	total kinematic acceleration, ft/sec^2

$\mathbf{v}$	linear input vector
v	aircraft y-body axis velocity, ft/sec
$\dot{v}$	aircraft y-body axis kinematic acceleration, ft/sec^2
$\mathbf{W}$	inverse linearizing transformation
$\mathbf{w}$	noise
w	aircraft z-body axis velocity, ft/sec, noise
$\dot{w}$	aircraft z-body axis kinematic acceleration, ft/sec^2
X_T	thrust in the aircraft x-body axis, lb
$\mathbf{x}$	state vector
$\dot{\mathbf{x}}$	state time derivative vector
$\tilde{\mathbf{x}}$	state vector of the apparent linear plant
x	north inertial position, ft
Y	aircraft total sideforce, lb
$\mathbf{y}$	measurement vector
y	east inertial position, ft
Z_T	thrust in the aircraft z-body axis, lb
z	vertical inertial position, ft
α	angle of attack, deg
$\dot{\alpha}$	angle of attack rate, deg/sec
β	angle of sideslip, deg
γ	wind reference frame Euler pitch angle, deg
$\Delta n_{z_{com}}$	commanded incremental load factor, g
ϵ	engine orientation angle, deg
η	throttle, deg
η_{com}	commanded throttle, deg
θ	body reference frame Euler pitch angle, deg
$\dot{\theta}$	body reference frame Euler pitch angle rate, deg/sec
ϕ	body reference frame Euler roll angle, deg
$\dot{\phi}$	body reference frame Euler roll angle rate, deg/sec
ω	rotational rates, deg/sec
$\dot{\omega}$	rotational accelerations, deg/sec^2

Subscripts

a	aerodynamic
a_n	body axis normal accelerometer output
b	body axis
br	body axis relative to inertial system

D	derivative
h	altitude
I	integral
k	kinematic
M	Mach number
m	measurement feedback system
P	proportional
p	power–configuration model
p	nonlinear plant system; power
q	body axis pitch rate
r	position
ref	reference value
u	function of the input
V	total velocity
v	estimate or model output
x	function of the state
y	output
0	initial conditions, or zero altitude
α	angle of attack
ϕ	body reference frame Euler roll angle

BACKGROUND

The motivation for using direct nonlinear flight-control synthesis techniques for designing aircraft autopilots and guidance systems is that these techniques are not limited by their reliance on linear perturbation models of the aircraft. While linear design techniques easily handle linear or nearly linear systems, as system nonlinearities become more pronounced, the effort required to design guidance laws increases rapidly. Although linear techniques are still capable of addressing such problems, a new technique is desired that would handle the nonlinearities simply and more directly.

The flight-test trajectory control problem [8,9,10,11] is a particular type of guidance problem that faces these issues. Flight-test maneuvers often cover ranges of the flight envelope, encountering aerodynamic and thrust nonlinearities. In some cases, the maneuvers specified are themselves nonlinear trajectories such as windup turns and pushover–pullups. These effects increase the complexity required from a linear design technique.

Flight-Test Trajectory Control

In flight-test trajectory control, the requirement is to provide precise, repeatable control of an aircraft during maneuvers used to gather aerodynamic, structural, propulsion, and performance data. For conventional flight regimes these maneuvers are fairly straightforward and, in general, easily modeled. Level-accelerations–decelerations, pushover–pullups, and windup turns are typical of these maneuvers. The original motivation in developing pilot-aiding displays for the open-loop problem [9] and closed-loop controllers for automatic maneuvering [8,10,11] was to increase the quality of flight data and to ensure repeatable, consistent maneuvers.

Numerous approaches to the flight-test trajectory problem were taken including cut-and-try techniques on a nonlinear simulation [9], linear optimal control [12,13,14], optimal cooperative control [15], eigenstructure assignment [13,16,17], suboptimal output feedback [12], and classical control theory [11]. Although successful open-loop and closed-loop systems were developed and used in flight, each of these approaches had limitations. The open-loop flight-test trajectory guidance (FTTG) was used on a number of aircraft programs [9] and was developed using a cut-and-try approach on piloted, nonlinear simulations. The success of the FTTG suggested that even better results could be obtained using a closed-loop controller, and the flight-test maneuver autopilot (FTMAP) was developed for the highly maneuverable aircraft technology (HiMAT) vehicle using classical control methods [8,10,11]. However, while there were successful applications of solutions to the flight-test trajectory control problem, none of the design techniques employed in the development of these systems were adequate in terms of providing a concise methodology for developing outer-loop controllers.

Except with the FTTG, all of the problems of transforming from a linear to a nonlinear system were encountered and an extensive cut-and-try session was needed to adjust the controllers when they were implemented and tuned using a nonlinear simulation. Furthermore, because the most difficult flight-test maneuvers have significant coupling between axes, the tuning problem was more than simply the iterative adjustment of parameters within a single control loop; simultaneous adjustment of parameters in multiple control loops was required. The use of nonlinear control [2,3] simplifies many of these problems, although some cut-and-try tuning is still required.

Deriving linear perturbation models of aerodynamics and propulsion systems [18,19] as well as inner-loop, flight-control systems is a difficulty facing the engineer using design methods based on linear perturbations. Perhaps an even more formidable problem that arises in using linear perturbation methods for FTTCs is the requirement for a large number of design cases and, hence, perturbation models. In addition to the requirements imposed because aerodynamic forces and moments change as a function of flight conditions, varying degrees of cross-axis coupling often must be accounted for at each flight condition. These additional requirements add significantly to an already complex design problem.

Nonlinear Control

Meyer and Cicolani [4] describe a formal structure for advanced flight-control systems that provides the basis for the results described in this paper. This formal structure may now be taken as preliminary results that motivated a large body of work in nonlinear controls and inverse model theory. This formal structure included features that were assumed in later applications:

1. A block triangular system was assumed,
2. inner- and outer-loop control functions were not explicitly separated,
3. a time-scale separation (hierarchy) was assumed (either explicitly or implicitly),
4. inverse aerodynamic and thrust models were used to provide an "open-loop, *a priori*" feedforward control, and
5. the feedforward control included an inverse model of the aircraft and control system dynamics.

This formal structure, the total automatic flight-control system (TAFCOS), has been applied in detailed nonlinear simulations of the de Havilland C-8A Buffalo augmentor wing jet short takeoff and landing (STO) research aircraft (AWJSRA) [20,21], and a vertical attitude takeoff and landing (VATO) aircraft [22,23,24]. The TAFCOS has also been used in flight tests on a DHC-6 Twin Otter aircraft [25,26], the AWJSRA [5], and a UH-1H helicopter [7,27]. Excellent results were achieved in all of these studies and the claim made by Meyer *et al* [27] that "the method is effective for a large class of dynamic systems that require multiaxis control and that have highly coupled nonlinearities, redundant controls, and complex multidimensional operational envelopes" can be taken as thoroughly validated.

Parallel to the cited work on TAFCOS, Meyer, Hunt, and Su [6,7,28,29,30,31,32,33] have pursued research in the underlying theory of linearizing transformations by model inversion. Necessary and sufficient conditions for the existence of transformations from nonlinear to linear systems were established by Su [32] and Hunt *et al* [30]. These transformations were shown to be global results by Hunt *et al* [30]. Meyer [6] and Meyer *et al* [7] have described a general structure (fig. (1)) for automatic control based on these results. This structure contains transformations (the WT-map) which when taken with the aircraft, provide a linear system that is modeled in the 'MODEL SERVO.' The reference trajectory, $\mathbf{r}^*$, is fed into the 'MODEL LAW' which determines the required input for the linear system to follow that trajectory. The regulator then determines the input required for the W-map using the linear input, $\mathbf{v}_0$, the linear states, $\mathbf{y}_0$, and the apparent linear system state feedback, $\mathbf{y}$.

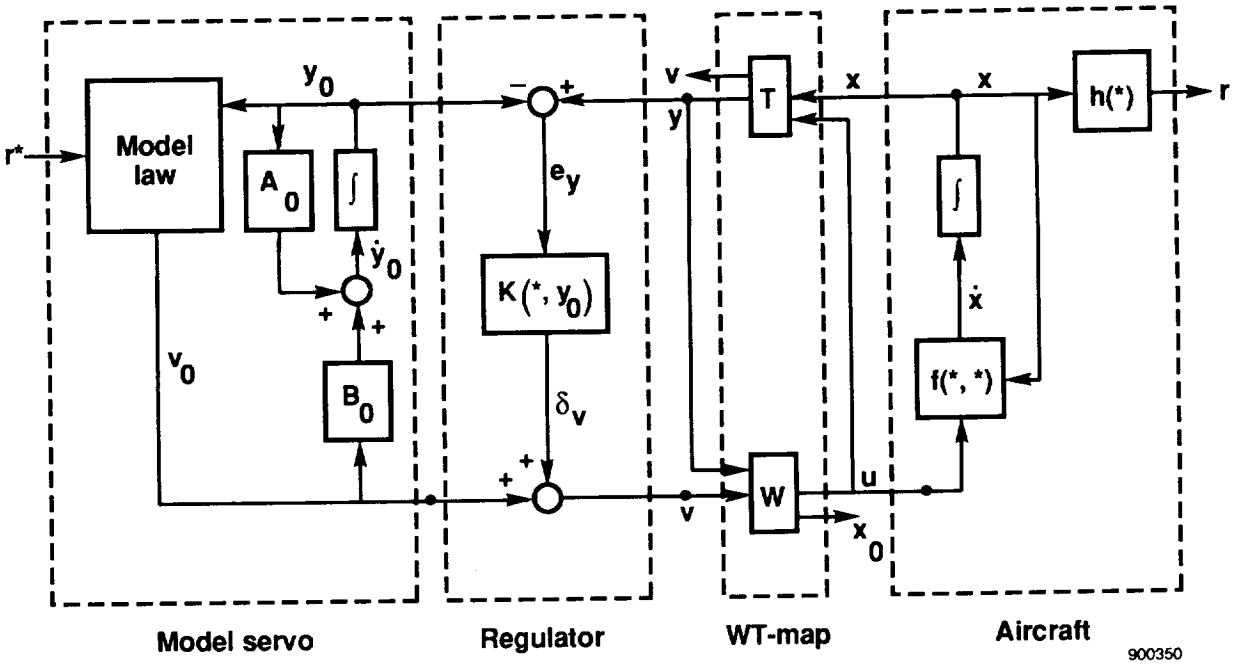

Figure 1. Meyer's formal structure for advanced flight-control systems.

In this structure, a general nonlinear system equation of the form

$$\dot{\mathbf{x}}(t) = \mathbf{f}[\mathbf{x}(t), \mathbf{u}(t)] \tag{1}$$

with the state $\mathbf{x} \in \Re^n$, the control $\mathbf{u} \in \Re^m$, and $\mathbf{f} : \Re^n \times \Re^m \rightarrow \Re^n$, an analytic function is assumed. Because it is a necessary condition for such a system to be transformable to a controllable linear system [27], it is assumed that equation (1) can be reformulated as an equivalent system in terms of new state and control coordinates $\mathbf{x}$ and $\mathbf{u}$ so that the system is in the form

$$\dot{\mathbf{x}}(t) = \mathbf{f}[\mathbf{x}(t)] + \sum_{i=1}^{m} \mathrm{u}_i(t)\mathbf{g}_i[\mathbf{x}(t)] \tag{2}$$

with

$$\mathbf{f}(0) = 0 \tag{3}$$

This nonlinear system is transformed using a mapping $T : \Re^n \rightarrow \Re^k \times \Re^l$, called the "T-map," such that

$$\begin{bmatrix} \mathbf{y} \\ \mathbf{v} \end{bmatrix} = T(\mathbf{x}, \mathbf{u}) \tag{4}$$

with $\mathbf{y} \in \Re^k$, $\mathbf{v} \in \Re^l$, where $\mathbf{y}$ and $\mathbf{v}$ are consistent with the state and control vectors of a time-invariant, linear system of the form

$$\dot{\mathbf{y}}_0(t) = A_0\mathbf{y}_0(t) + B_0\mathbf{v}_0(t) \tag{5}$$

This linear system model is used to determine reference inputs, $\mathbf{v}_0$, into a form compatible with the linear control law component of the linear controller ("REGULATOR" in fig. (1)). The linear system in equation (5) is sometimes referred to as the "reference model" and the elements of $\mathbf{v}$ in the linear, transformed system are known as "pseudocontrols."

An inverse T-map (sometimes referred to as a W-map) maps the pseudocontrols of the linear system, $\mathbf{v}$, into the nonlinear system inputs, $\mathbf{u}$, with $T^{-1} \equiv W : \Re^k \times \Re^l \rightarrow \Re^n$ such that

$$\mathbf{u} = W(\mathbf{y}, \mathbf{v}) \tag{6}$$

Also shown in figure 1 is a linear regulator that provides feedback control for the linear system with

$$\delta\mathbf{v} = \mathrm{K}\, e_{\mathbf{y}} \tag{7}$$

$$\mathbf{v} = \mathbf{v}_0 + \delta\mathbf{v} \tag{8}$$

$$e_{\mathbf{y}} = \mathbf{y} - \mathbf{y}_0 \tag{9}$$

The linear reference model, shown as the "MODEL SERVO" in this figure, provides feedforward control for the total nonlinear control system. The nonlinear aircraft model to be controlled ("AIRCRAFT" block in fig. (1)) is presented by Meyer [6] and shown in figure 2. In this model, the aircraft is broken into three blocks: power/configuration, rotation, and translation. Basically, Meyer's aircraft model is a full state, six degree-of-freedom model, but has no inner-loop control system associated with it.

A simple example of a nonlinear controller designed to fly a level acceleration test maneuver is derived in appendix A.

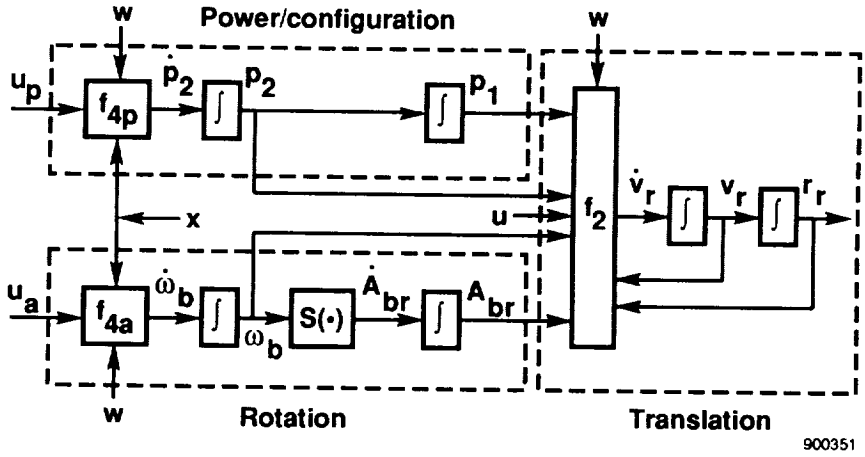

Figure 2. Meyer's generic aircraft model.

Application of Nonlinear Control to the Flight-Test Trajectory Control Problem

Menon *et al* [2] report the development of a nonlinear controller for the F-15 aircraft flight-test trajectory control problem. In this report, the time-scale separation implicitly assumed by Meyer and Cicolani [4,5] is made explicit using forced singular perturbation theory. A new model for the nonlinear controller is derived from these results.

The structure of this nonlinear controller is shown in figure 3. Time-scale separation allows the designer to separate the aircraft states into groups based on the dynamics of those states. If there is sufficient separation, the designer can develop a control law for the slower states while assuming the faster states have no dynamics. That is, if the closed-loop plant (inner-loop control system and vehicle) is fast enough to achieve the condition commanded by the outer-loop before the outer-loop guidance system computes a new command, the closed-loop plant will be seen to have reduced or no dynamics by the outer-loop. This technique provides the designer a simpler system around which to build a control system. For example, figure 3 shows the aircraft states separated into very fast states–servo actuator states, fast states p, q, and r (typically inner-loop states), and slow states V, h, α, β, θ, and ϕ (typically outer-loop or guidance states). In fact, there is yet a slower group of states x, and y (used in navigation). The outer-loop guidance system must be slow enough to let the plant achieve the commanded states before updating guidance commands. The states can be separated into different groups depending on the requirements of the task.

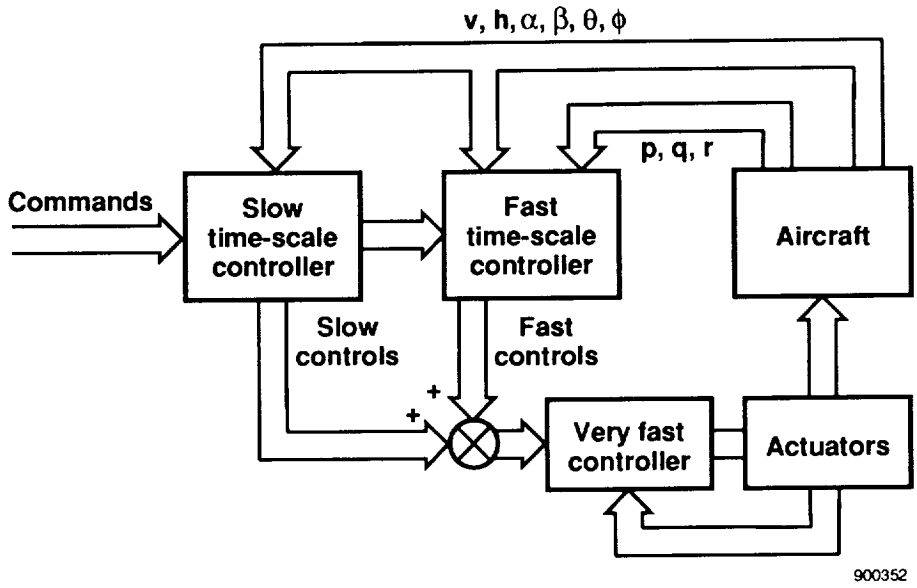

Figure 3. Separation of fast and slow time-scale controllers.

Menon *et al* [3] provide a detailed derivation of nonlinear flight-test control laws based on the results of Menon *et al* [2] in which the outer-loop flight-test control outputs are fed into an inner-loop CAS. In this latter report, the explicit time-scale separation from Menon *et al* [3] is made implicit, because the CAS is assumed to be much faster than the flight-test control. Excellent results were obtained when this flight-test control was tested using a nonlinear six-degree-of-freedom simulation containing detailed, full-envelope models of the F-15 aerodynamics, propulsion system, and control system. While this work is based on the use of detailed aerodynamic models in the nonlinear control, it forms the basis for the application of nonlinear control to the outer-loop control problem addressed by the current work.

A NEW APPROACH TO THE NONLINEAR CONTROL PROBLEM

It will be demonstrated in the following that the requirement for detailed aerodynamic models in nonlinear control laws can be eliminated by using accelerometer and rate gyro outputs. This simplifies the nonlinear controller in two ways

1. Aerodynamic force calculations are not required in the controller, and

2. the nonlinear controller to a large extent becomes "model independent" given the same command paths into the inner-loop control system.

Both of these features provide the potential for major design, implementation, and execution time benefits. The model-independence feature is perhaps the most significant contribution, because it offers the possibility of designing a generic, general-purpose outer-loop control law *that is independent of the aircraft to which it will be applied.* Obviously, complete model independence can only be achieved when one can represent vehicles by identical models. For the controller derived and implemented in this paper, only nonlinearities due to aerodynamics and equations of motion are considered. While other nonlinearities exist, they are not accounted for and are a likely cause of some of the problems observed in the controller. These are nonlinearities in the inner-loop control system such as stick mass inertia, and command scaling. Such nonlinearities contribute to the dependence of the controller on the aircraft model.

Conceptual Structure for Nonlinear Control Law Design

The nonlinear control laws developed for the FTTC are based on the generic model of the aircraft for outer-loop control shown in figure 4 rather than Meyer's generic aircraft shown in figure 2. The primary difference is that while the technique of Meyer *et al* provides for direct control of surface displacement to control rotation of the aircraft in pitch and roll, the technique used in the FTTC relies on the CAS to provide surface displacement controls to achieve the commanded values of roll rate and incremental load factor.

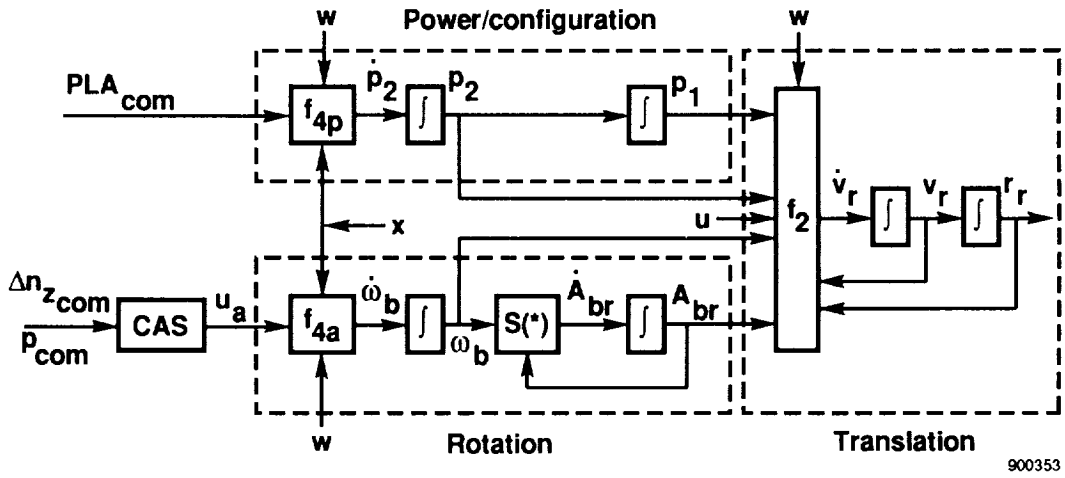

Figure 4. Generic model of aircraft for outer-loop control problem.

The structure used to develop the nonlinear control laws for the FTTC is shown in figure 5. This structure differs from the formal structure for advanced flight-control systems introduced by Meyer [6,7] and shown in figure 1. The structure used for the FTTC uses states based directly on the measured (or reconstructed) aircraft states rather than the error between the linear model and the linear system (aircraft and WT-map). The advantages of the current approach are that determining the apparent linear system (described later) is fairly straightforward and potential for poor tracking due to modeling error is significantly reduced.

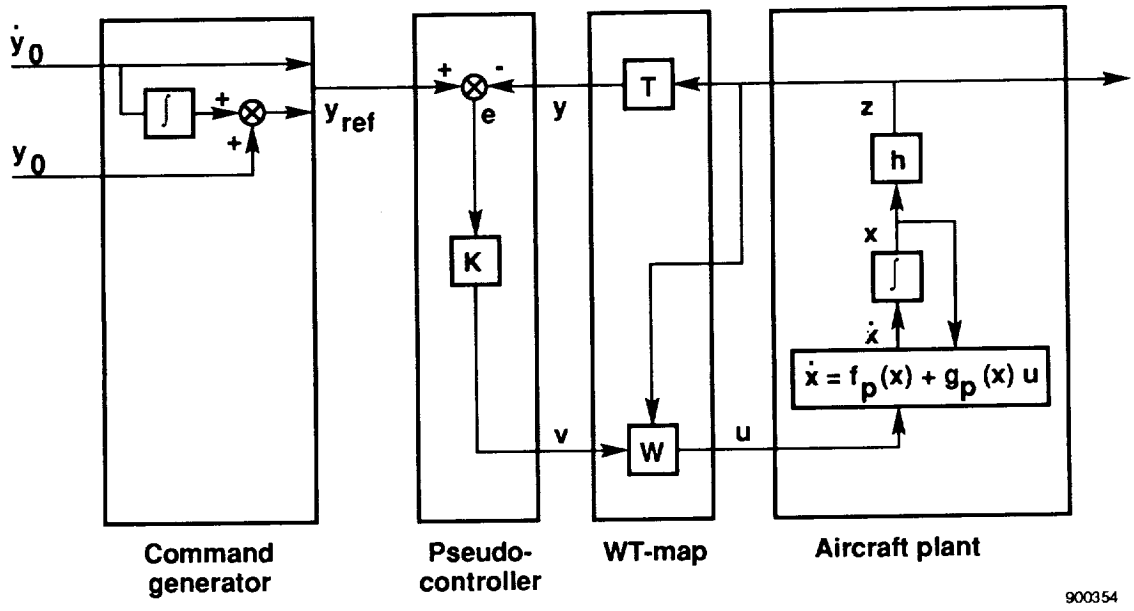

Figure 5. Structure used for flight-test trajectory control (FTTC).

A significant difference between Meyer's formal structure and the one used for the current work is that the nonlinear plant in Meyer's structure is assumed to consist of only nonlinear state equations whereas the current work assumes a measurement equation

$$\mathbf{z} = \mathbf{h}(\mathbf{x}) \tag{10}$$

The T-map for the structure shown in figure 5 is defined as

$$\mathbf{y} = \mathrm{T}(\mathbf{z}) \tag{11}$$

however, most often, T is just the identity matrix. The T-map for Meyer's controller shown in figure 1 is given by equation (4).

$$\begin{bmatrix} \mathbf{y} \\ \mathbf{v} \end{bmatrix} = \mathrm{T}(\mathbf{x}, \mathbf{u})$$

The W-map for the nonlinear controller shown in figure 1 is defined by

$$\mathbf{u} = \mathrm{W}(\mathbf{y}, \mathbf{v}) \tag{12}$$

Whereas, the W-map for the FTTC is

$$\mathbf{u} = \mathrm{W}(\mathbf{v}, \mathbf{z}) \tag{13}$$

While the difference could be reconciled by stating that the measurement function $\mathbf{h}(\mathbf{x})$ is included in the T-map, there is a subtle difference in that the values in the measurement vector are generally obtained straight from aircraft sensors, not computed.

Linear and Nonlinear System Formulations

The plant around which the FTTC is designed includes the aircraft, the CAS and actuators, and the instrumentation system. This plant is modeled by the equation

$$\dot{\mathbf{x}} = \mathbf{f}_p(\mathbf{x}) + \mathbf{g}_p(\mathbf{x})\mathbf{u} \tag{14}$$

$$\mathbf{z} = \mathbf{h}(\mathbf{x}) \tag{15}$$

In this model, the number of states must be the same as the number of controls.

When taken with the WT-map (inverse linearizing transforms) and ignoring the fast dynamics of the CAS and other components by applying time scale separation, the system can be rewritten as being linear with the following formulation

$$\dot{\tilde{\mathbf{x}}} = A\tilde{\mathbf{x}} + B\mathbf{v} \tag{16}$$

This formulation is known as the *apparent linear plant.* When properly developed, this system is in the Brunovsky canonical form. The state vector $\tilde{\mathbf{x}}$ includes relevant states selected from the nonlinear system as well as the required integral states.

Derivation of the Linearizing Transformation

The input to the apparent linear system, $\mathbf{v}$, is defined as

$$\dot{\mathbf{x}} = \mathbf{v} \tag{17}$$

This equation and equation (14) are then combined so that

$$\mathbf{v} = \mathbf{f}_p(\mathbf{x}) + \mathbf{g}_p(\mathbf{x})\mathbf{u} \tag{18}$$

This is the linearizing transform for state feedback.

Next, the terms $\mathbf{f}_p(\mathbf{x})$ and $\mathbf{g}_p(\mathbf{x})$ in equation (15) must be transformed into terms that are functions of the measurement vector, $\mathbf{z}$

$$\mathbf{f}_p(\mathbf{x}) = \mathbf{f}_m(\mathbf{z}) \tag{19}$$

$$\mathbf{g}_p(\mathbf{x}) = \mathbf{g}_m(\mathbf{z}) \tag{20}$$

So that equation (14) becomes

$$\dot{\mathbf{x}} = \mathbf{f}_m(\mathbf{z}) + \mathbf{g}_m(\mathbf{z})\mathbf{u} \tag{21}$$

This transformation eliminates the need for aerodynamic models in the linearizing transformations of systems developed previously. The linearizing transformation as a function of measurements is given by

$$\mathbf{v} = \mathbf{f}_m(\mathbf{z}) + \mathbf{g}_m(\mathbf{z})\mathbf{u} \tag{22}$$

Each real control input into the plant can then be separately determined by solving equation (22) for each nonlinear input u_i so that

$$u_i = g_{mi}(\mathbf{z})^{-1}\left[v_i - f_{mi}(\mathbf{z})\right] \tag{23}$$

This equation represents the W-map which is the inverse linearizing transformation for the real input to the nonlinear system found in figure 5. The T-map in the same figure maps the plant outputs (measurements) to the linear system outputs. In this formulation, the T-map is identity. Implicit in this equation is the assumption that $g_{mi}(\mathbf{z}) \neq 0$.

Linear Control Law Design

In the formulation of the FTTC, the linear control law is a simple tracker as opposed to the explicit model follower used by Meyer *et al* [7]. The linear control law or pseudocontrol receives its input, $\mathbf{e}$, from the feedback, $\mathbf{y}$, of the apparent linear system and the reference or command trajectory, $\mathbf{y}_{ref}$, so that

$$\mathbf{e} = \mathbf{y}_{ref} - \mathbf{y} \tag{24}$$

For the tracker, the first step of the design is to determine the nature of the command to be used (that is, step, ramp, or parabola). From this, the designer can determine the number of integrators required for the control law. Once this has been established, the pseudocontrol gains can be determined from the apparent linear system using modern or classical control techniques.

Nonlinear System Equations

For the aircraft described in figure 4, if the inner-loop control states are ignored, the aircraft can be represented by a nonlinear system equation in the form of equation (2)

$$\dot{\mathbf{x}}(t) = \mathbf{f}[\mathbf{x}(t)] + \mathbf{g}[\mathbf{x}(t)]\mathbf{u}(t) \tag{25}$$

with

$$\mathbf{x} = \begin{bmatrix} V \\ \alpha \\ \phi \\ \theta \\ \dot{h} \end{bmatrix} \tag{26}$$

For a given maneuver, three states to be controlled are selected from these five states. The controls for this system are the inputs to the inner-loop controller, and are defined for this application to be

$$\mathbf{u} = \begin{bmatrix} \mathrm{u}_1 \\ \mathrm{u}_2 \\ \mathrm{u}_3 \end{bmatrix} = \begin{bmatrix} \Delta n_{z_{com}} \\ p_{com} \\ \eta_{com} \end{bmatrix} \tag{27}$$

where

$$\Delta n_{z_{com}} = a_{n_{com}} - 1 \tag{28}$$

The nonlinear system state equations used are the standard wind axis equations of motion which correspond to the states in the state vector and can be found in reference [34]. They are

$$\dot{V} = \frac{1}{m}[\, -D\cos\beta + Y\sin\beta + X_{\mathrm{T}}\cos\alpha\cos\beta + Z_{\mathrm{T}}\sin\alpha\cos\beta - mg(\cos\alpha\cos\beta\sin\theta - \sin\beta\sin\phi\cos\theta - \sin\alpha\cos\beta\cos\phi\cos\theta)\,] \tag{29}$$

$$\dot{\alpha} = \frac{1}{Vm\cos\beta}[-L + Z_{\mathrm{T}}\cos\alpha - X_{\mathrm{T}}\sin\alpha + mg(\cos\alpha\cos\phi\cos\theta + \sin\alpha\sin\theta)] + q - \tan\beta(p\cos\alpha + r\sin\alpha) \tag{30}$$

$$\dot{\phi} = p + q\sin\phi\tan\theta + r\cos\phi\tan\theta \tag{31}$$

$$\dot{\theta} = q\cos\phi - r\sin\phi \tag{32}$$

$$\ddot{h} = \frac{1}{gm}[\sin\theta(X_{\mathrm{T}} - D\cos\alpha + L\sin\alpha) - (Y)\sin\phi\cos\theta - \cos\phi\cos\theta(Z_{\mathrm{T}} - D\sin\alpha - L\cos\alpha)] - 1 \tag{33}$$

These equations assume the acceleration of gravity remains constant and side force due to thrust is zero. Of these, equations (31) and (32) are already in measurement feedback form. Equations (29), (30), and (33) need to be transformed into measurement feedback form. This is done in appendix B, where the linearizing transforms are derived.

If we assume that a maneuver begins at $t = t_0 = 0$ with the aircraft at the trimmed state, so that $\dot{\mathbf{x}} = 0$, then equation (25) can be written as

$$\dot{\mathbf{x}}(0) = 0 = \mathbf{f}[\mathbf{x}(0)] + \mathbf{g}[\mathbf{x}(0)]\mathbf{u}(0)$$

If we define the inputs for the trim condition to be $u_i(0) = 0$ for $i = 1, 3$, then it follows that

$$\mathbf{f}[\mathbf{x}(0)] = 0$$

Extensions to the General Trajectory Control Problem

Kato and Sugiura [35] present results for the general trajectory problem that, like the results presented herein, are based on the work of Meyer *et al* [4,5,26]. In their article they apply transformations from the wind-reference-frame Euler angles to the body-reference-frame Euler angles to show how a general reference trajectory can be controlled using nonlinear control. These results are related to those presented by Cicolani and Weissenberger [36].

The results of Kato and Sugiura combine the inner- and outer-loop control and transform a general flight trajectory specified in terms of position variables into vehicle surface commands using the basic nonlinear control methods and aerodynamic models. As has been shown in the present paper, the need for these aerodynamic models can be eliminated from the outer-loop control law using measurement feedback. It is unclear whether the present results can be extended to the inner-loop problem. Further research will address this topic.

From the point of view of outer-loop control, the problem of navigation requires looking at the aircraft as a point in a known inertial system. Although this problem is not addressed directly in this paper, there are no obvious reasons why this approach would not work adequately for this purpose. The use of another layer on the outer loop may be required, as well as the addition of the inertial position states (x, y, and z), to the system equations.

Control Laws

The control laws for the nonlinear FTTC are driven by error signals obtained by computing the difference between the linear state vector and the reference state vector prescribed by the desired aircraft trajectory. The output of these linear control laws are pseudocontrols which are transformed, using the W-map, into commands for the aircraft–inner-loop system.

There are three different trajectories contained in the FTTC: a level acceleration maneuver, a pushover–pullup maneuver, and an excess-thrust windup turn maneuver. The level acceleration maneuver is a wings level, constant altitude maneuver with Mach number increasing (or decreasing) at a specified rate. The pushover–pullup maneuver is a wings level, constant throttle maneuver with angle of attack varying at a specified rate from trim to a minimum value then to a maximum value then back to trim. The excess-thrust windup turn is a constant altitude, constant Mach maneuver with angle of attack increasing at a specified rate to a specified value.

The control laws used for the implementation discussed later in this paper are described here. A complete derivation of each of the control laws shown in the following three subsections is found in appendix B. Basically, there are three command loops available to be controlled by the FTTC. These are pitch, which is controlled by incremental load factor command, $\Delta n_{z_{com}}$; roll, which is commanded by roll rate command, p_{com}; and thrust, which is controlled by throttle command, η_{com}. This is not to say that these are the only commands for which control laws may be developed, but that these are the commands required by the implementation used to validate this approach. It would be fairly simple to develop control laws to meet other command requirements.

Pitch Control Laws

The pitch commands for the FTTC are computed using two different control laws and transformation equations. The level-acceleration–deceleration maneuver uses an altitude command; the excess-thrust windup turn and the pushover–pullup maneuver use an angle-of-attack command.

The intermediate command of vertical acceleration is computed in the altitude command pitch loop using the following linear control law

$$\ddot{h}_{com} = k_{h_D} e_{\dot{h}} + k_{h_P} e_h + k_{h_I} \int_{t_0}^{t_f} e_h dt \tag{34}$$

with

$$e_{\dot{h}} = \dot{h}_{ref} - \dot{h}$$

$$e_h = h_{ref} - h$$

Then $\Delta n_{z_{com}}$ is obtained from $\ddot{h}_{com}$ using the inverse linearizing transformation equation (appendix B, eq. (B-28))

$$\Delta n_{z_{com}} = -1 + \frac{\ddot{h}_{com} - a_x \sin\theta + a_y \sin\phi \cos\theta + 1}{\cos\theta \cos\phi} \tag{35}$$

The second pitch control is the angle-of-attack command loop. The linear control law for this loop is

$$\dot{\alpha}_{com} = k_{\alpha_P} e_\alpha + k_{\alpha_I} \int_{t_0}^{t_f} e_\alpha dt \tag{36}$$

where

$$e_\alpha = \alpha_{ref} - \alpha$$

From $\dot{\alpha}_{com}$ an intermediate pitch rate command is computed using the inverse linearizing transformation (appendix B, eq. (B-59))

$$q_{com} = \dot{\alpha}_{com} + \tan\beta(p\cos\alpha + r\sin\alpha) - \frac{1}{V\cos\beta}[-g(a_n\cos\alpha + a_x\sin\alpha - \cos\alpha\cos\phi\cos\theta - \sin\alpha\sin\theta)] \tag{37}$$

The pitch rate command q_{com} is then used to determine the $\Delta n_{z_{com}}$ using the following inverse linearizing transformation (appendix B, eq. (B-54))

$$\Delta n_{z_{com}} = -1 + a_n + \frac{V\cos\beta}{g\cos\alpha}(q_{com} - q) \tag{38}$$

These two transformations could be combined into one transformation, however, the pitch rate command generated by equation (37) must be filtered because of noise and system delays. This effect is discussed in the Implementation Experience section. The separation of these equations is left in here for clarity.

Roll Control Laws

The lateral commands for the FTTC are computed using two different control laws and transformations. For the level-acceleration–deceleration and pushover–pullup maneuvers, the reference roll attitude ϕ_{ref} is known and $\dot{\phi}_{com}$ is computed using the linear control law

$$\dot{\phi}_{com} = k_{\phi_P} e_\phi + \int_{t_0}^{t_f} k_{\phi_I} e_\phi dt \tag{39}$$

where

$$e_\phi = \phi_{ref} - \phi$$

and p_{com} is computed using the inverse linearizing transformation equation (appendix B, eq. (B-70))

$$p_{com} = \dot{\phi}_{com} - \tan\theta(q\sin\phi + r\cos\phi) \tag{40}$$

The control law computation for the excess-thrust windup turn requires the use of two layers of outer-loop controllers. Each outer loop must be slower than its inner loop. For this control loop, the outer-loop linear control law computes an $\ddot{h}_{com}$ using the same linear control law shown in equation (34). Roll attitude command is then computed using the following inverse linearizing transformation equation (appendix B, eq. (B-81))

$$\phi_{ref} = -\cos^{-1}\left(\frac{a_x\sin\theta - \ddot{h}_{com} - 1}{\cos\theta\sqrt{a_y^2 + a_n^2}}\right) - \tan^{-1}\left(\frac{a_y}{-a_n}\right) \tag{41}$$

This intermediate command is used in the linear control law

$$\dot{\phi}_{com} = k_{\phi_P}e_\phi + \int_{t_0}^{t_f} k_{\phi_I}e_\phi dt$$

from which p_{com} is computed using the inverse linearizing transformation equation (40).

Thrust Control Laws

Two throttle commands were required for the maneuvers defined. The first simply holds the throttle position constant at the current or some predefined position

$$\eta_{com} = \eta_{ref}$$

The throttle command for all other maneuvers is computed using the linear control law

$$\dot{M}_{com} = k_{M_D}e_{\dot{M}} + k_{M_P}e_M + \int_{t_0}^{t_f} k_{M_I}e_M dt \tag{42}$$

where

$$e_{\dot{M}} = \dot{M}_{ref} - \dot{M}$$

$$e_M = M_{ref} - M$$

which is used to establish a thrust command T_{com} from the inverse linearizing transformation equation (appendix B, eq. (B-114))

$$T_{com} = \frac{1}{\cos\alpha\cos\beta}\{ma\dot{M}_{com} - gm[a_y\sin\beta + \cos\beta(a_x\cos\alpha - a_n\sin\alpha)] - X_T\cos\alpha\cos\beta + mg(\cos\alpha\cos\beta\sin\theta - \sin\beta\sin\phi\cos\theta - \sin\alpha\cos\beta\cos\phi\cos\theta\} \tag{43}$$

The actual throttle setting is determined by using a model of the thrust–throttle relationship (without dynamics) and inverting it so that

$$\eta_{com} = f_T^{-1}(h, V, T_{com}) \tag{44}$$

The thrust term X_T in equation (43) is obtained using the same model with a simple lag to simulate the engine lag.

Control Law Coupling

The inverse transformation described in equation (23) transforms output feedback and linear controls to the nonlinear inputs required by the nonlinear plant. This transform provides a decoupled connection between the linear control law and the nonlinear plant. However, by decoupling the CAS inputs, errors caused by command limits and rate limits can be introduced to the inputs. For instance, if the vertical acceleration guidance law commands a load factor greater than the 4.0-g limit, the Mach guidance law linearizing transformation would get an erroneous input for normal acceleration. In addition to the limits problem, for decoupling, a different three-axis guidance law (with corresponding linearizing transformations) would be required for each maneuver. This adds complexity to the programmers task. Layering of outer-loop guidance laws presents another problem because, although the layers for each command path are separated in time scale, it is not necessarily the case that there is separation of time scales between the inner layer of one path and the next layer of another path.

The solution chosen for this application is to treat equation (23) as a scalar equation, and to feed back the measured values of the terms that are inputs to other guidance paths. This way, limits and other nonlinearities in one path do not affect another, although there is some delay associated with this method. This solution also simplifies the programmer's task in that there is only one inverse transform required for each command and maneuvers that have identical guidance laws in any one particular channel (such as the angle-of-attack rate guidance law used by both the windup turn and pushover–pullup) can use the identical piece of code.

SYSTEMS DESCRIPTION

The next three subsections describe the systems and software used to develop, evaluate, and test this approach. As has been stated before, the theory and control laws developed in this paper are of generic application. There is no requirement to use a specific aircraft or type of aircraft to implement them. The control laws were developed for an aircraft which accepts incremental load factor, roll rate, and PLA commands. It should be clear, however, that similar control laws could be developed to meet almost any command requirements, because the approach would remain the same. The feedback gains selected should, however, keep the aircraft capabilities in mind. Therefore, no effort will be made to give an in-depth description of the systems used. Instead, descriptions will be given to provide adequate information regarding how the experiment was performed, and to describe drawbacks which had or were expected to have noticeable impacts on the results of the experiment.

Simulation Development System Description

The system on which the FTTC was developed and evaluated is shown in figure 6. It consists of two computers; the simulation computer and the control law computer. The simulation computer contains a six-degree-of-freedom nonlinear simulation of the F-15 HIDEC aircraft with full-envelope aerodynamic and thrust models, F-15 CAS and actuator models, and atmospheric and sensor models. The simulation computer also contains a simulation of the discretization effects and pure delays of the actual flight system. The control law computer contains only the FTTC software. The two computers communicate with each other through dual-port shared memory. This system is designed to simulate, as accurately as possible, the remotely augmented vehicle (RAV) system. The RAV system, on which the controller was flown, is described in the next section.

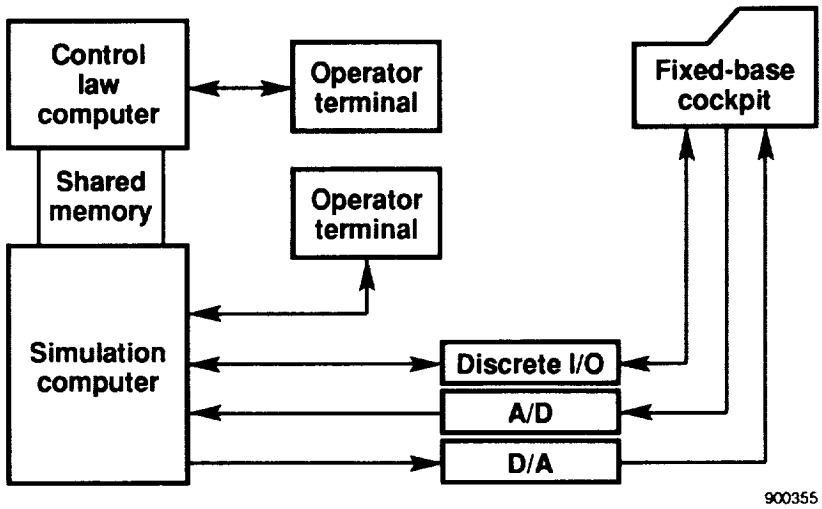

Figure 6. FTTC simulation development and evaluation system.

Simulation sensor information is taken from the simulation and passed through a simulation of the discretization effects and pure delays of the RAV downlink telemetry system before it is passed through shared memory to the FTTC. The FTTC uses the simulated sensor information, user-defined maneuver specifications and the control laws described earlier to compute commands to be sent back to the simulation. These commands are passed back through shared memory and go through a simulation of the uplink telemetry discretization effects and pure delays. The values are then passed to the F-15 CAS model in the simulation computer. The simulation computer integrates the equations of motion. Results are then displayed on instruments in a fixed-base cockpit, recorded to disk, or recorded on a strip chart. The simulation and controller are monitored and controlled by operator terminals attached to each computer.

This system allows development and evaluation of the FTTC by engineers and pilots. It also provides an effective means for software validation, flight system verification and validation, and flight test.

The simulation is a very good representation of the flight system with two exceptions. First, the simulation runs at a rate of 50 Hz. While this is fine for representing the aircraft aerodynamics, it is two and a half times as fast as the actual aircraft onboard systems which run at a rate of 20 Hz. However, the simulation in its current configuration cannot be operated at 20 Hz. It is possible that aircraft response may vary from simulation response for this reason. This was not expected to have a large effect on the flight-test results.

The second item is sensor noise and bias. While the aircraft sensors are meticulously calibrated, it is impossible to eliminate the noise of the sensed data without increasing the loop delay of the overall system. It is also very difficult to model the noise and bias of the sensors in the simulation system. This was expected to have a noticeable effect on the flight system.

Flight-Test System Description

The F-15 HIDEC aircraft and the RAV system shown in figure 7 were used to flight test the control laws. The F-15 HIDEC aircraft is a preproduction F-15 with Pratt and Whitney 1128 engines (Pratt and Whitney, West Palm Beach, FL), a digital CAS, and a digital electronic engine control (DEEC) computer [1]. The RAV system has both

downlink and uplink capabilities, and has a ground-based minicomputer in which control laws may be implemented for flight test. This system eliminates the need for large computational capabilities onboard the aircraft.

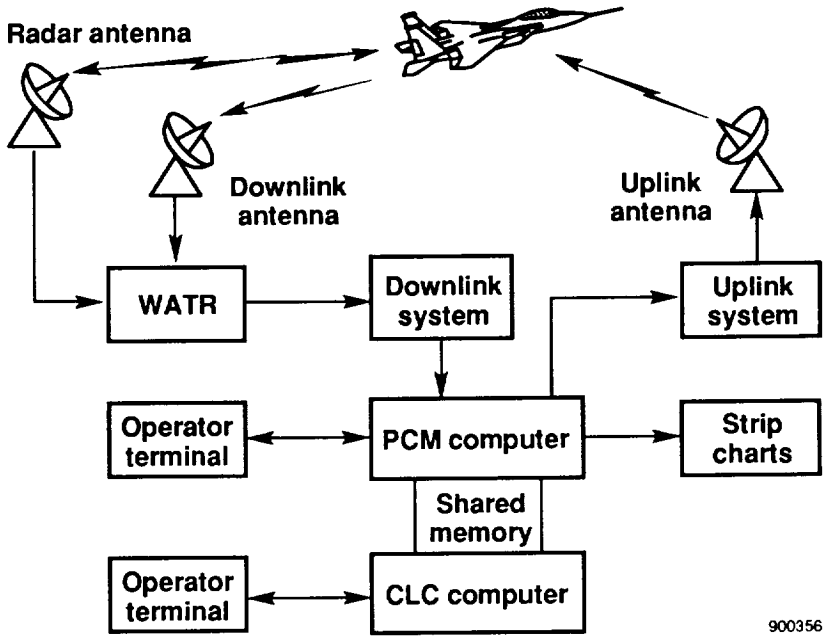

Figure 7. Remotely augmented vehicle (RAV) system used to flight test the FTTC.

The RAV system is designed so that software developed and tested on the control law computers of the simulation systems may be transported directly and run on identical computers in the RAV system. In fact, it is a requirement that no changes be made between the software tested on the simulations and the software used in flight. This enables the engineer to perform verification and validation tests cheaply and easily on the simulation before using the aircraft and RAV system which have limited availability and cost much more to operate.

The drawback, however, is that an additional 80 to 100 msec of pure delay are added to the control loop. This delay added to an aircraft system delay caused by the asynchronous systems of up to three frames (or up to 150 msec), can make the control task much more difficult if not impossible. For the FTTC, this was expected to cause a noticeable problem since part of the fast controller–the linearizing transform–resides in the ground system.

The allowable command ranges for the controller were set to be ± 150.0 deg/sec in roll rate, -0.75 to $+4.0\ g$ in incremental load factor ($+0.25$ to $5.0\ g$ normal acceleration), and full range for both throttles.

Flight-Test Trajectory Control Software Program

The linear control laws and nonlinear inverse transformations described in the Control Laws section were implemented in FORTRAN in a computer program called FTTC, along with a command generator to produce the reference time histories of the states to be tracked. An operator interface to the controller was developed to input maneuver specifications and to monitor the FTTC and flight-test system.

This program is designed to run in the control law computer in the simulation and RAV systems. The basic frame time of the program is 12 msec. However, only the maneuver selection logic and the linearizing transformations run at this rate. The command generator and pseudocontroller run every other frame. This is done because the command generator and the pseudocontroller really represent the outer-loop controller (slow controller in fig. (3)), while the

linearizing transformations and the CAS form the inner-loop controller (fast controller in fig. (3)). The linear system to be controlled is represented by the linearizing transformations, CAS, and aircraft together.

The frame time was selected because it was the fastest that the software could run without getting frame overruns. A slower frame time would have added to the overall loop delay of the system. However, this means that the controller sees constant values of sensed data between downlink data frames which have the same rate as the aircraft system (50 msec). This could become a problem during very dynamic maneuvers.

DISCUSSION

It is important to note that in the nonlinear control laws defined by equations (34) through (44), none of the equations use aerodynamic terms and, hence, none of these control laws require aircraft-specific aerodynamic models. In fact, no aircraft-specific models are required except for the simple thrust-throttle mapping shown in equation (44). These results are significant in their differences from the results reported by previous authors. In those results, expressions for lift, drag, and side force would appear in the equations in place of the accelerometer output terms.

Thus, the claim of model-independence is shown to be valid under two main assumptions:

(1) the generic model of the combined aircraft inner-loop control system (fig. (4)) is a reasonable representation of the actual system, and

(2) the time-scale separation of the inner- and outer-loop control laws is a reasonable approximation.

This somewhat ignores the inverse thrust-throttle mapping. However, it is anticipated that the need for using this mapping can be eliminated using an additional feedback loop; this development will be the subject of future research.

During simulation and flight test, controller performance was measured by the ability to keep aircraft parameters within specified tolerances. These tolerances are

$\pm .01$ Mach number,

± 100 ft altitude, and

$\pm 0.3°$ angle of attack.

In addition to these, it is required that the controller have smooth transitions from the capture of initial conditions to the beginning of the maneuver itself. Also, when parameters to be tracked are ramped, the controller is to maintain the tolerances while ramping those parameters smoothly. The large tolerance in angle of attack is due to the noise and accuracy problems associated with the measurement of that parameter.

Simulation Results

Figure 8 shows the time history from a simulated level-acceleration maneuver from Mach 0.75 to Mach 1.20 at 25,000 ft. The command rate for this maneuver is $\dot{M}_{com} = 0.01\, sec^{-1}$. The plots show that Mach number increases smoothly and that throttle command is smooth throughout the acceleration. Altitude and roll attitude are also held relatively constant (less than ± 10 ft and $\pm 1.0°$, respectively) during the maneuver. This maneuver spans a range of dynamic pressure from 309 lb/ft^2 to 793 lb/ft^2. This represents a large Mach range spanning well more than half of the flight envelope. This also represents a range of conditions over which the aircraft can in no way be represented linearly.

Figure 9 shows the time history from a simulated pushover–pullup maneuver at Mach 0.90 and 10,000 ft (825 lb/ft^2 dynamic pressure). The maneuver is initiated from a wings-level, trim condition. Angle of attack is commanded

at a rate of $\dot{\alpha}_{com} = -0.5$ deg/sec from trim α first to $\alpha = 0°$ and then at a rate of $\dot{\alpha}_{com} = +0.5$ deg/sec to $\alpha = 2.5°$. During the maneuver, throttle is held constant and roll attitude is commanded to remain wings level. The plots show smooth ramping of angle of attack throughout the maneuver. However, angle of attack never reaches the condition of 0° because the commanded incremental load factor reaches its lower limit before that condition is attained. On the other hand, the angle of attack never reaches the desired maximum condition of 2.5° because the integrator in the angle-of-attack pseudocontrol has wound up while the commanded incremental load factor was limited. By the time the command generator starts the pushover from the maximum angle-of-attack condition, the aircraft has not yet achieved 2°. Neither the proportional nor the integral part of the linear control law can act fast enough or have great enough magnitude to eliminate this error. The reason is that the CAS does not provide an exact linear control of measured load factor based on commanded incremental load factor. This is discussed further in the Implementation Experience section.

Figure 10 shows the time history of a simulated excess-thrust windup turn at Mach 0.65 and 25,000 ft, which corresponds to a dynamic pressure of 232 lb/ft^2. This maneuver begins at the straight-and-level-trim condition and increases angle of attack to 12° at a rate of 1 deg/sec. Altitude is maintained to within $\pm$60 ft. Mach number is held to within $\pm$.02 until the end of the rollout back to trim. This error, which is in excess of the specified tolerance, is caused by a 1.5-sec delay built into the throttle command to eliminate the problem of the throttle toggling between core power and afterburner. It is expected that if this delay were not required, Mach number would have been maintained within the tolerance. For this maneuver, the aircraft longitudinal, lateral, and thrust controls are coupled because of the relatively high angle of attack and steep roll attitude. But while the controller handles this level of coupling adequately, there are indications that problems may exist at slower speeds or higher angles of attack. Each time the angle-of-attack control changes between a steady-state control and a ramp control, the roll controller has difficulty controlling altitude. However, up to this level of coupling, the controller's performance during this maneuver demonstrates that this approach handles this problem.

Figure 11 shows the time history from a simulated excess-thrust windup turn at Mach 1.2 and 25,000 ft. This maneuver reaches an angle of attack of 5°. The plots show that altitude is held to within 40 ft and Mach to within Mach 0.005. For this maneuver, dynamic pressure is 793 lb/ft^2. The performance of the controller during these two windup turns proves that the controller is capable of fairly precise control over a large range of dynamic pressures (232 lb/ft^2 to 793 lb/ft^2) *without changing control law gains.*

In fact, simulation evaluation was conducted across a Mach number range from 0.60 to 1.20 and across an altitude range from 10,000 ft to 40,000 ft, with acceptable results except at the high and slow conditions. While these results did not fall within the specified tolerances, the controller was still able to perform the maneuver. It is expected that the slower, higher flight conditions which have still lower dynamic pressures may be a problem because the aircraft dynamics get slow enough to invalidate the assumption of time-scale separation between the inner- and outer-loop controls.

Simulation tests were also conducted with varying amounts of pure delay in the uplink and downlink simulation. Total system delays ranging from 120 to 240 msec were examined over a matrix of maneuvers simulated at Mach 0.75 and 1.20 and at altitudes of 10,000 ft, 20,000 ft, 30,000 ft, and 40,000 ft. The controller performed acceptably at all conditions, with the same exceptions indicated in the previous paragraph.

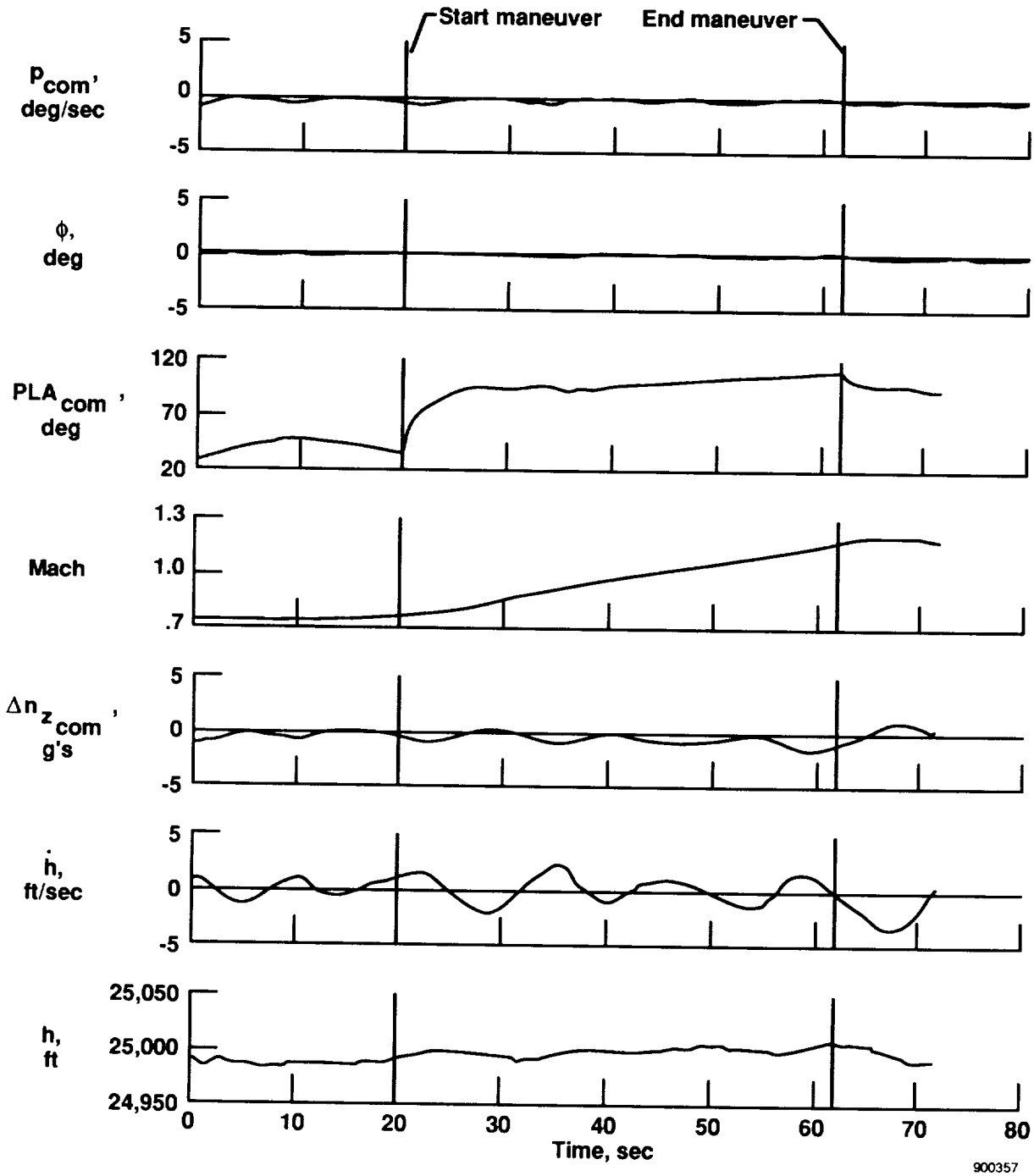

Figure 8. Simulated level-acceleration maneuver from Mach 0.75 to Mach 1.20 at 25,000 ft.

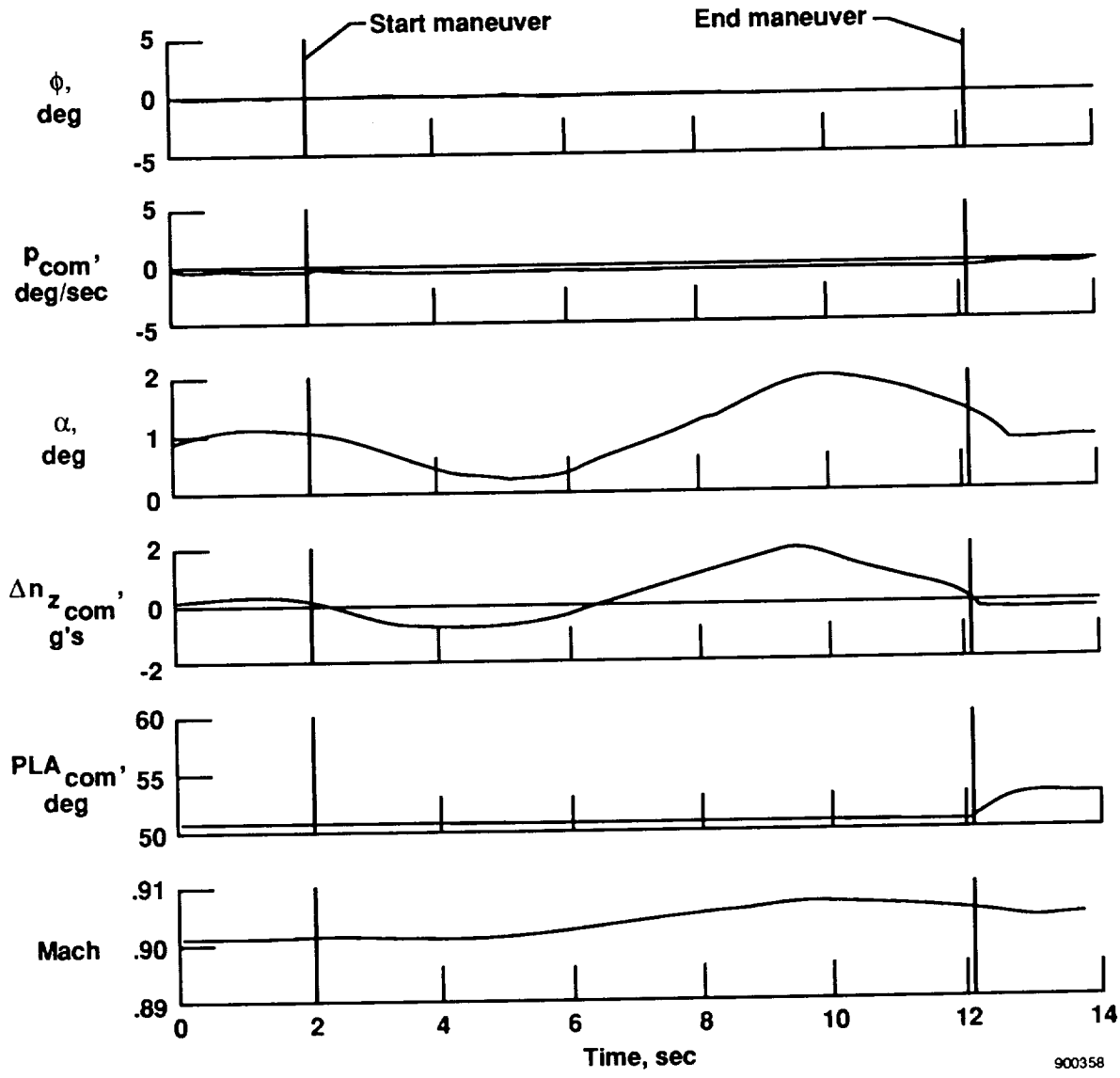

Figure 9. Simulated pushover–pullup maneuver with angle of attack varying between $\alpha = 0°$ and $\alpha = 2.5°$ at Mach 0.90 and 10,000 ft.

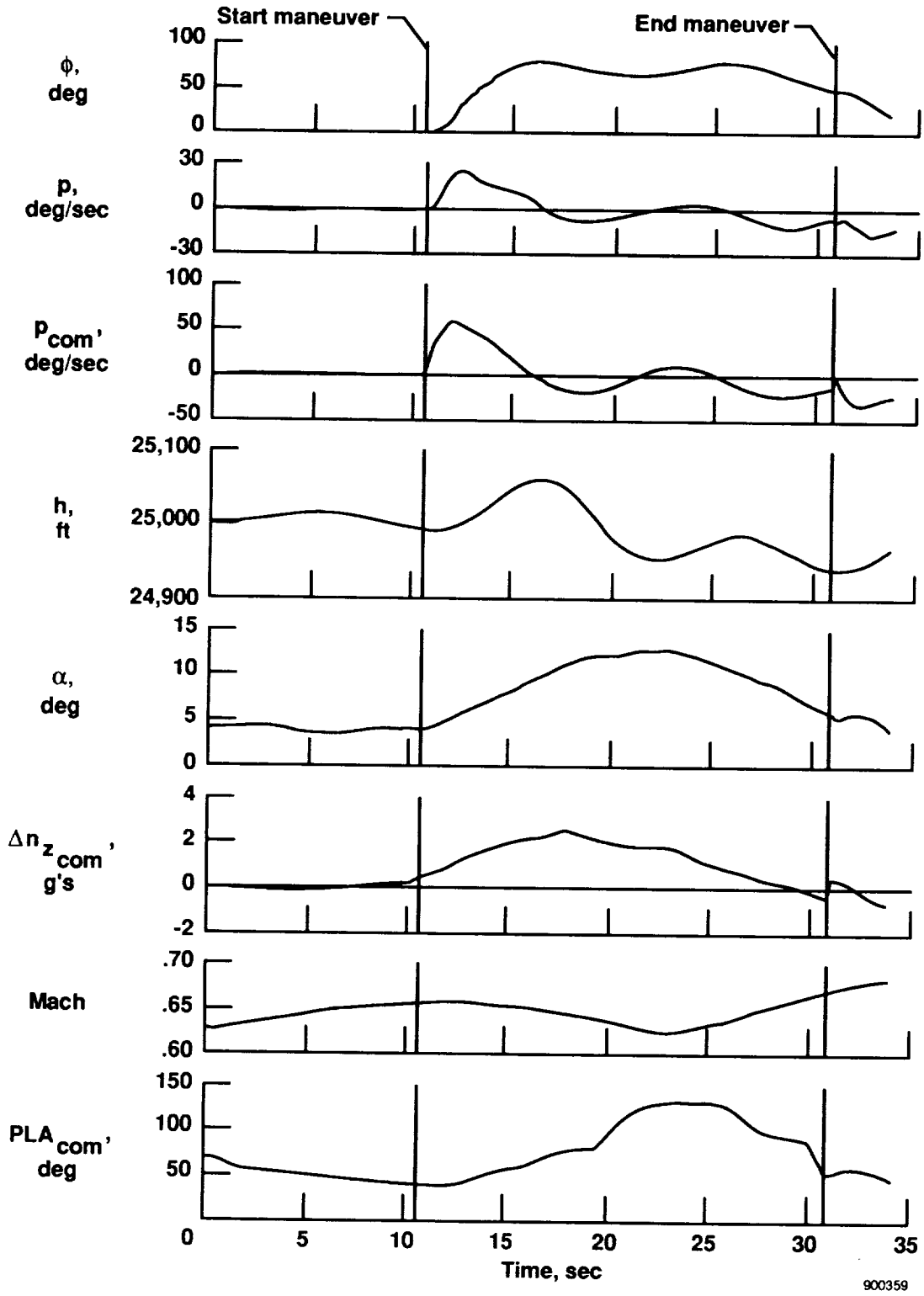

Figure 10. Simulated excess-thrust windup turn to $\alpha = 12°$ at Mach 0.65 and 25,000 ft.

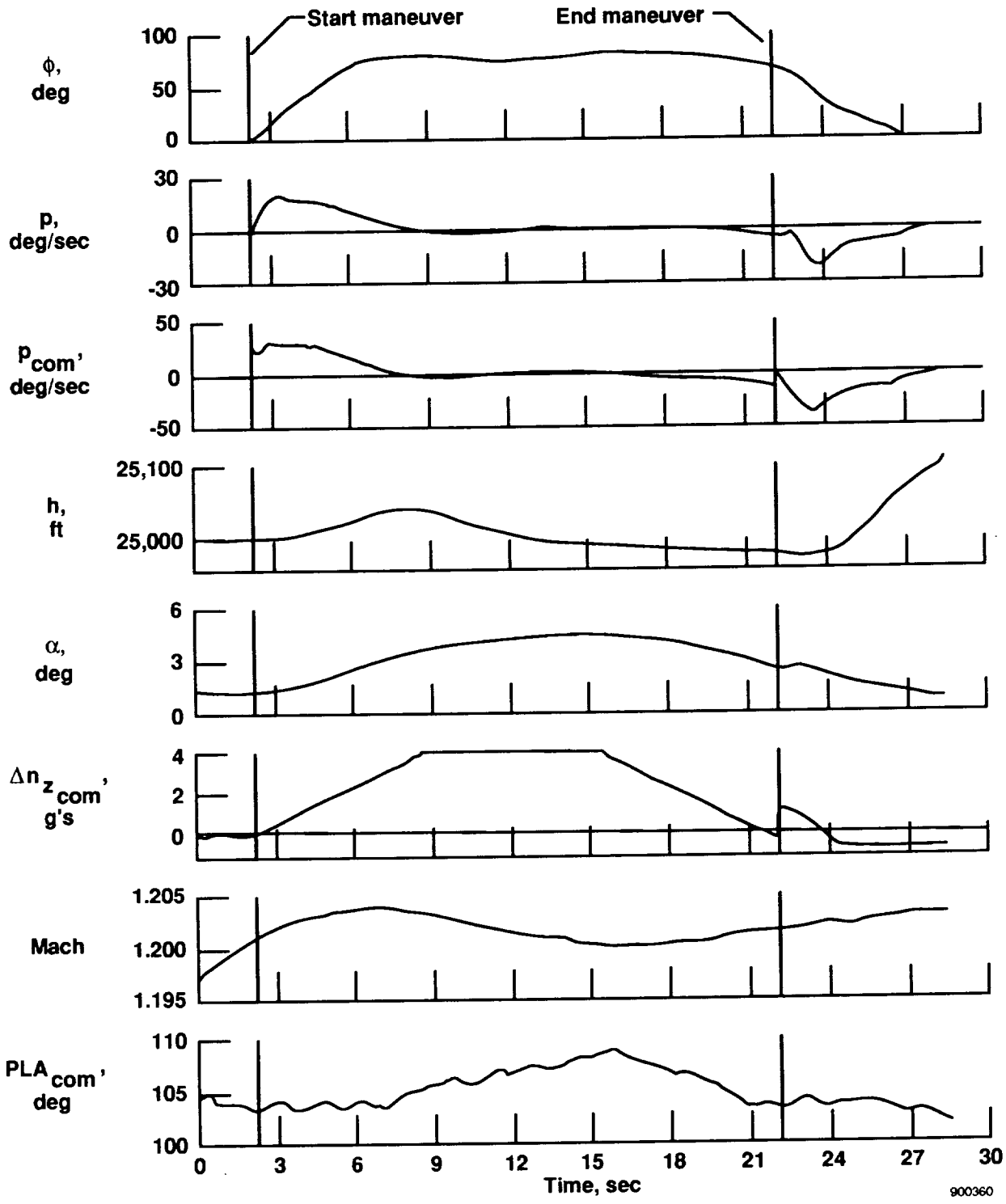

Figure 11. Simulated excess-thrust windup turn to $\alpha = 4°$ at Mach 1.20 and 25,000 ft.

Flight-Test Results

The FTTC was flown between June and August, 1989. During these flights, pseudocontroller gains were adjusted and minor changes were made in the control law to improve performance of the controller. These gain changes were required primarily because of nonlinearities in the aircraft CAS that were not accounted for in the controller and because of measurement noise. The controller did fulfill the expectations of providing adequate control of the aircraft over a large range of flight conditions, although some work was still required to get the quality of results expected. Four of the maneuvers flown are presented in figures 12 through 15 and are discussed here.

The first maneuver, which is shown in figure 12, is a level acceleration maneuver from Mach 0.70 to 1.20 at a rate of 0.01 Mach number per second. The roll attitude is held relatively constant with an error of less than 2.0°. Mach number increases at a constant rate except for a short time around Mach 1.0 (at approximately the 30-sec mark). This effect is caused by sensor error as the shock wave forms at the tip of the nose boom.

A much larger transonic effect can be seen in the altitude, altitude rate, and commanded incremental load factor plots. The cause of phenomena seen in these plots can be traced to the source of these measurements. The altitude and altitude rate measurements are taken from the inertial navigation system on the F-15 aircraft. Inertial altitude rate is derived by filtering and integrating a set of accelerometer and rate gyro inputs. Therefore, it is not affected by the shock wave across the pitot-static system on the airplane. However, inertial altitude is obtained by integrating the value of altitude rate and removing accumulated biases by comparing inertial altitude with the altitude from the static pressure system while the aircraft is in nearly unaccelerated flight (that is, level flight). Hence, as the aircraft passes through the transonic regime, the altitude tends to decrease because of the sensed increase in static pressure before the shock. The inertial system filters this information into its estimate of altitude. The resulting value is sent down to the controller which attempts to correct by climbing. The reverse occurs as the aircraft achieves supersonic flight and the static system is behind the shock wave. This is the cause of the apparent discrepancy between altitude and altitude rate in the time histories. However, the inertial system is slow in filtering the pressure altitude into the inertial altitude, so the effect, while noticeable, is fairly small and leads to an altitude error of approximately ± 60 ft.

The pushover–pullup maneuver shown in figure 13 was flown at Mach 0.90 and 10,000 ft with angle of attack varying between 0° and 2.5° at a rate of 0.5 deg/sec. Angle of attack is tracked well in this maneuver although sensor noise does affect the commanded value noticeably. From these time histories, it is difficult to determine whether the noise in the sensed angle-of-attack trace (which is unfiltered) is caused by noise in the commanded incremental load factor trace, or vice versa. Other maneuvers were performed in which commanded incremental load factor remains constant yet there is still noise on the angle-of-attack trace. The problem of noise on angle of attack shows up in the next two maneuvers and will be discussed later in more depth.

Figures 14 and 15 show excess-thrust windup turns. The first one is flown at Mach 0.65 and 25,000 ft, while the second one is flown at Mach 1.20 and 25,000 ft. The maneuver at Mach 0.65 tracks altitude poorly with a maximum error of approximately 150 ft before it starts to roll out to straight and level. This maneuver also has difficulty tracking Mach number with an error of approximately $\pm .02$ Mach for the same reason as the simulated maneuver discussed in the last section. The level of control coupling caused by the angle of attack and steep roll attitude presents a greater problem to the controller in the flight system than in the simulation system. This coupling along with the throttle delay contributes to the large altitude excursion.

The second excess-thrust windup turn, which is performed at Mach 1.20, does not show the pitch and thrust coupling problem. In fact, altitude is kept to within ± 25 ft, and Mach number is kept to within $\pm .008$ of the commanded value. Here, however, angle of attack is not ramped smoothly to the desired value of 5°, and even though the commanded incremental load factor is at its maximum value, the angle of attack measured is just over 3°. This problem and a similar one between commanded and measured roll rate will be discussed in the Implementation Experience section.

The roll racheting effect was the effect during flight test which the pilots found least acceptable, and in some cases unacceptable. This effect can be seen at the beginning of the roll into the turn. Roll racheting varied in magnitude and frequency depending on the conditions of the turn. In the slower or higher turns the effect was not noticeable to the pilot. The origin of this effect is unclear. While it did not show up in the simulation evaluation of the system as flown, it could be made to appear in several ways by varying gains, maneuver requirements, delays, etc. Therefore, no definite source was determined. This effect is also discussed further in the Implementation Experience section.

The origin of the noise in the angle of attack and commanded incremental load factor seen in the pushover–pullup maneuver can be explained, at least in part, by the maneuvers in figures 14 and 15. During both maneuvers, the commanded incremental load factor reaches its maximum limit and is held constant there for a short time. However, noise in the angle-of-attack trace is significant (up to approximately 0.3°) and is probably a result of either measurement noise, turbulence, or both. Angle of attack provides the feedback for the intermediate command of angle-of-attack rate (see eq. (36)), as well as heavily influencing the inverse transformation shown in equations (37) and (38). The commanded incremental load factor computation seems to amplify the noise on angle of attack. While this is not a divergent process, filtering sensed angle of attack will be necessary to provide smoother tracking of commanded angle of attack.

The results of the FTTC flight test indicate that the approach using linearizing transforms with measurement feedback is a valid approach for developing outer-loop controllers for nonlinear systems. Tracking reference trajectories is acceptable over a large range of altitudes and Mach numbers using only a single set of gains.

In general, the flight-test data matched the simulation data with the exception of sensor noise, which was not modeled in the simulation. The problem of roll ratcheting warrants further research.

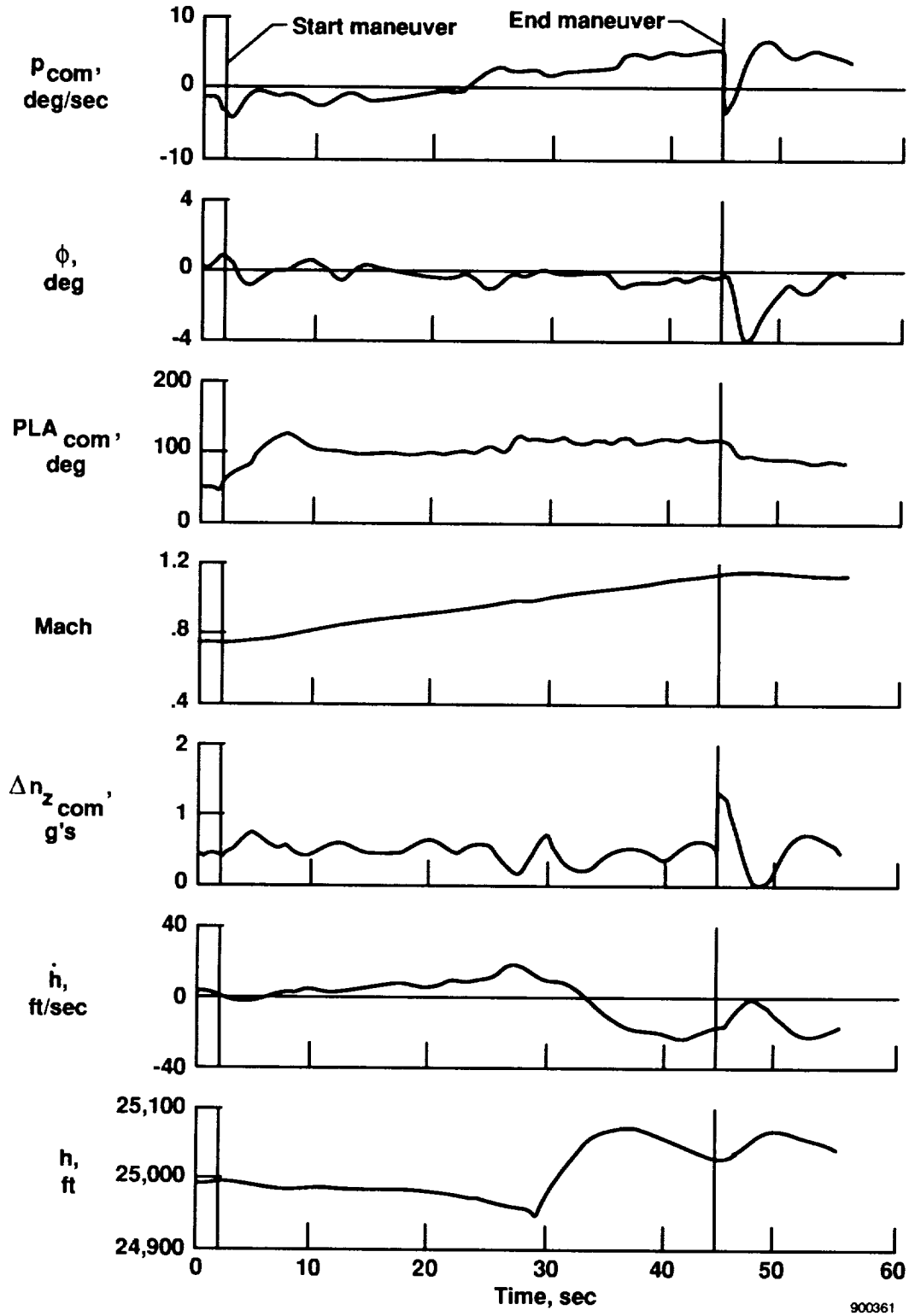

Figure 12. Flight data of a level acceleration maneuver flown from Mach 0.70 to Mach 1.20 at 25,000 ft.

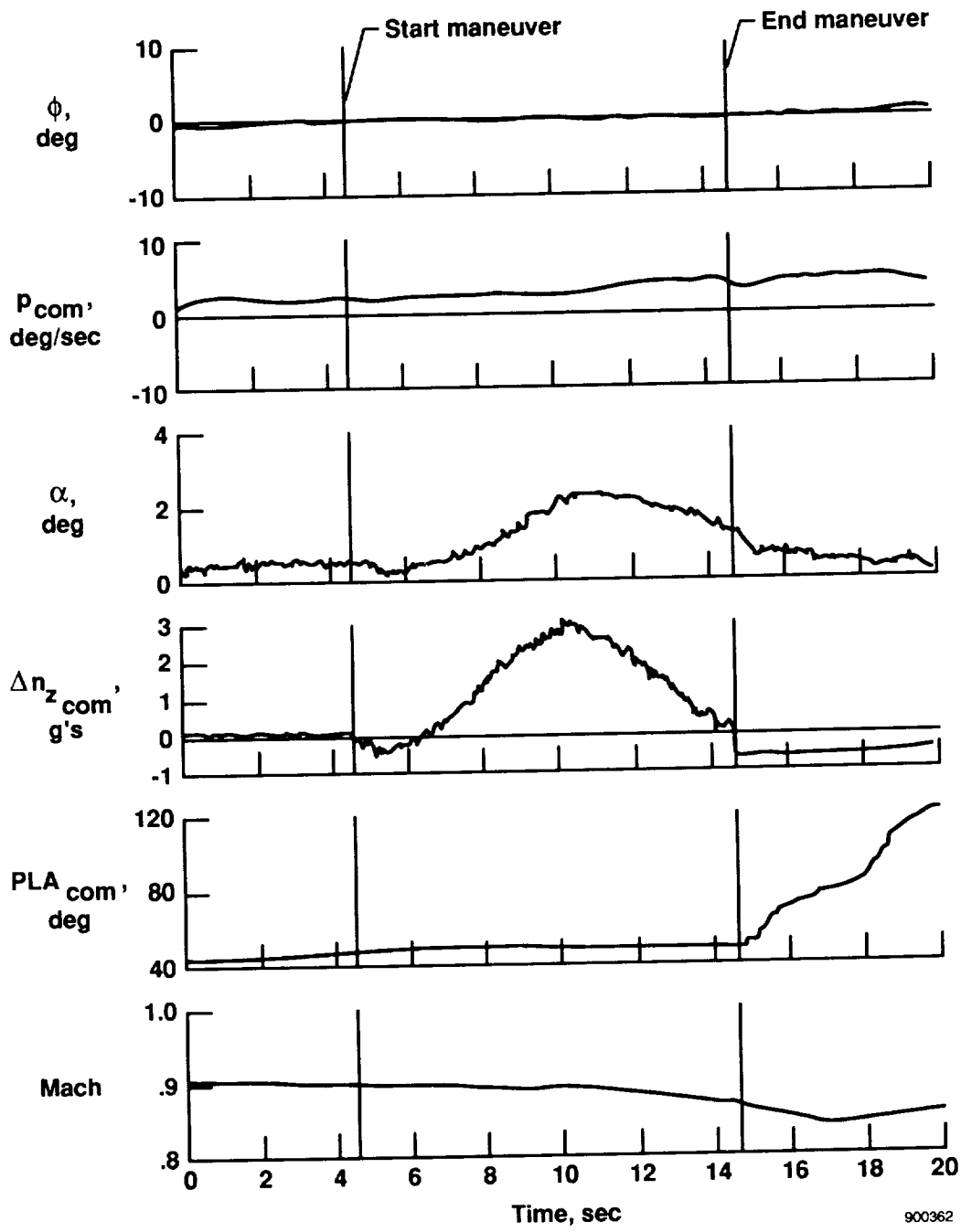

Figure 13. Flight data of a pushover–pullup maneuver flown at 10,000 ft, Mach 0.90 with angle of attack varying between $\alpha = 0°$ and $\alpha = 2.5°$.

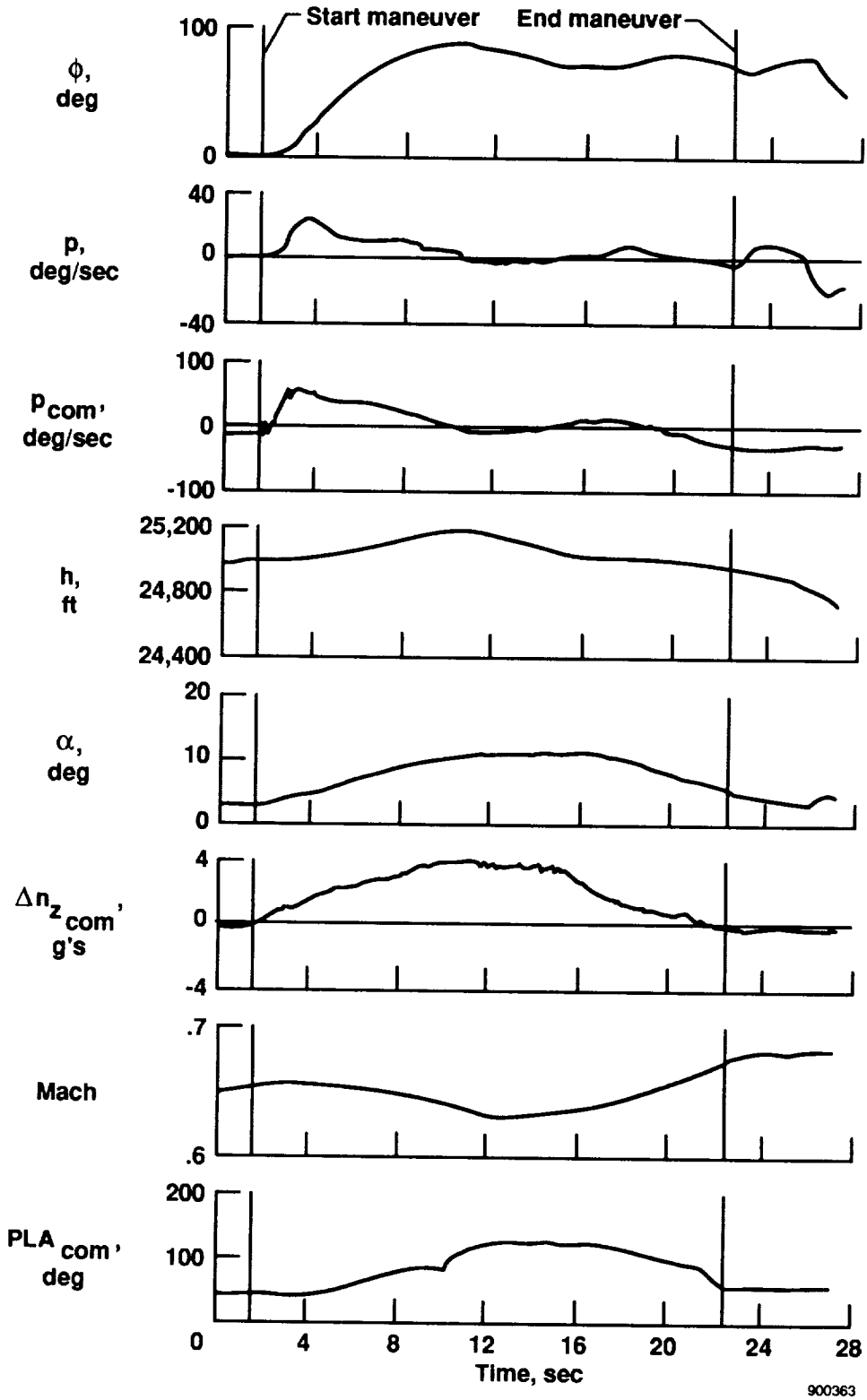

Figure 14. Flight data of an excess-thrust windup turn maneuver flown at 25,000 ft and Mach 0.65 from α_{trim} to $\alpha = 12°$.

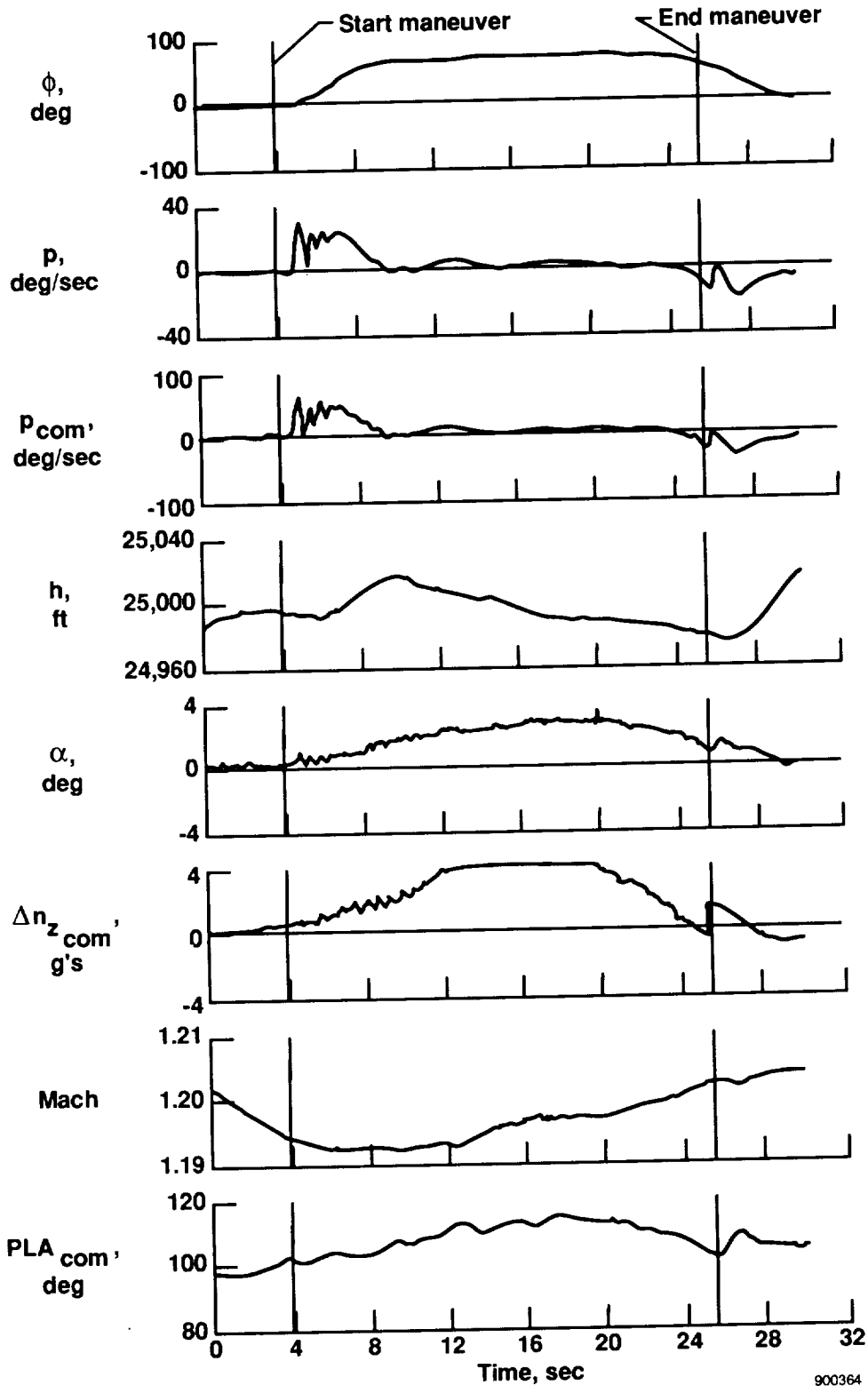

Figure 15. Flight data of an excess-thrust windup turn maneuver flown at 25,000 ft and Mach 1.20 from α_{trim} to $\alpha = 4°$.

Implementation Experience

There were several factors in the implementation that caused problems to the experiment. These factors are discussed here to provide some insight to problems which may be encountered in future implementations.

During the development, simulation, and flight test of the FTTC, some adjustments in gain values were required, although the objective was to develop a technique which would eliminate gain adjustments. At least part of the reason for this is the inaccuracy of the modeling of nonlinearities in the inverse transformations. While the transformations used account for the nonlinearities in the equations of motion and in the aerodynamics of the aircraft, they do not account for the nonlinearities in the aircraft control system. One example of this is discussed later in this section when the roll ratcheting problem is examined. Further research is required to determine if modeling these nonlinearities actually minimizes gain adjustments.

In this implementation, the F-15 CAS did not control the aircraft to provide the roll rate commanded by the FTTC. In fact, roll rate command was two and a half times as great as the achieved roll rate, as can be seen by the flight data from the turning maneuvers. Also, flight data indicate that this scaling factor is not constant, but varies slightly with flight condition. This might provide a partial explanation for the roll ratcheting problem discussed in the Flight-Test Results section, since it could cause the loop gain to be too high at some flight conditions. Additionally, the sensed and commanded roll rates from flight-test data do not compare to those from the simulation in terms of their relative magnitude. This points out that there is a modeling inaccuracy in the simulation. Such modeling inaccuracies explain the need to adjust gains once flight test is underway.

Flight data also indicate a similar scaling factor problem between incremental load factor and achieved load factor. This presents a problem in accurately tracking the reference parameter in the pitch axis, although there is no similar ratcheting problem in pitch. This along with the limited range in incremental load factor command significantly limits the capability of the controller to perform maneuvers.

As discussed in the Control Laws section, the same linear control law (eq. (34)) was used for altitude tracking in both the pitch and roll control loops. However, the actual implementation of these two control laws required different gains for each of the loops. While it is not obvious that this should be the case, examination of the control loops provides insight as to why this is necessary. The $\ddot{h}_{com}$ control law of the altitude commanded pitch control loop is fairly fast since it has only one outer loop. The $\ddot{h}_{com}$ control law of the altitude commanded roll control loop is designed to be slower since it is the outermost loop in a multilayered control loop and must observe the requirement of time-scale separation keeping it slower than any of the inner loops of this control.

The implementation of the control laws in the FTTC does not provide control decoupling for the reasons described in the Control Law Coupling section. As can be seen in the simulation and flight data of the maneuvers, this does not appear to be a problem. Very good performance is achieved in highly coupled maneuvers despite the decoupled inverse transformation equations. Coding is much simpler. Verification and validation testing is much less complicated and provides a higher level of confidence in the software.

As was discussed in the Flight-Test Results and Pitch Control Law sections earlier, one of the contributors to the noise in the angle-of-attack based incremental load factor command is the sensitivity of the intermediate q_{com} command to noise in measured angle of attack. The solution used here was to put q_{com} through a low-pass filter. The difference between q_{com} and measured q was then computed, and run through a proportional–integral control law to eliminate biases and standoff errors. The output of the proportional–integral control law would then be used in equation (38). This solution helped a great deal in eliminating high-frequency content of the command, and in improving tracking of the reference angle of attack. Another solution that was not tried would be to filter measured angle of attack. While this would eliminate the high-frequency content of the angle-of-attack signal, it would also add delay to the control loop. This was not tried because of the added delay.

One interesting unforeseen problem uncovered in the attempt to find the source of roll ratcheting was uncommanded stick movement. When a large step was input into the roll channel of the CAS in a turn, the aircraft rolled

sharply into the turn. The stick, because of its own inertia, would tend to resist the rolling motion, and put a roll command into the CAS in the opposite direction. This could cause the roll ratcheting effect experienced by the pilots and seen in the data. Maneuver conditions requiring less sharp changes in roll rate were attempted which reduced the ratcheting slightly. This effect and the command scaling effect in the roll and pitch command paths should be accounted for in the inverse transformation. However, it would be preferable to eliminate feedback through the control stick by setting stick commands to zero in the CAS while the system is engaged.

Comparison of Simulation and Flight-Test Results

The conditions of the simulation maneuvers and of the flight-test maneuvers (figs. (8) to (15)) were selected to provide a direct comparison between simulation and flight-test data. The only discrepancy is that the simulated level acceleration begins at Mach 0.70 while the level acceleration performed in flight starts at Mach 0.75.

While in general the simulation and flight-test results agree, it would clearly enhance the ability to analyze performance and select gains if the simulation were to run at the same rate that the aircraft systems run, and if the FTTC were to run at the same rate as the simulation or slower. In addition, modeling airdata noise in the simulation would have enabled the designer to fine tune the gains and the control laws for the flight system.

The level-acceleration maneuvers compare very well except for the transition through the sonic region in the flight data, which was discussed in the Flight-Test Results section. The transient at the end of the maneuver, as the controller flies the aircraft from the final condition of the maneuver to straight and level, unaccelerated flight, is much sharper in the flight data than during the simulation maneuver. The cause of the transient is the reset done in the pseudocontrollers when the controller switches from the maneuvering phase to the exit phase. During the exit phase, the controller recovers the aircraft to straight and level, unaccelerated flight. This reset is done to eliminate accumulated biases in the pseudocontrol laws enabling the controller to drive the aircraft to straight and level flight without first unwinding an integrator. The reason for the difference in transient magnitude between the simulation and flight data is that the aircraft has not recovered completely from the erroneous altitude data received while flying through the transonic region.

One other discrepancy can be seen in the incremental load factor command for each maneuver. For the simulated maneuver, the controller maintains zero or slightly negative values, while in flight test, the average value tends to be about 0.3 g. The probable cause for this is that the pilot had trimmed the aircraft slightly nose down and the controller was trying to eliminate this bias (which would be taken out by the integrator in the altitude pseudocontroller, causing the reset transient discussed in the previous paragraph).

The simulated windup turn at Mach 0.65 compares well with the flight tested turn. Mach and commanded PLA are nearly identical. However, there is no high-frequency content in the commanded roll rate for the simulated maneuver as there is in flight. This is probably because of noise in the measurements. In addition, while both trajectories achieve the target angle of attack, the simulated trajectory does not require nearly as much commanded incremental load factor. There is no clear explanation for this at this time.

Finally, the simulated and flight-tested windup turns at Mach 1.20 match rather well. The main difference is that the roll ratcheting seen in the flown maneuver is not seen in the simulated maneuver. Even so, the roll attitudes for the two maneuvers are similar, and the altitude time histories are also close. The differences in Mach number and commanded PLA are small and can be attributed to the fact that while the test-flown maneuver starts slightly above the specified initial Mach number, the simulated maneuver starts a little below the specified initial condition. The angle of attack and commanded incremental load factor are similar when noise and a slight difference in initial trim condition are considered.

CONCLUDING REMARKS

Research has been ongoing at the Dryden Flight Research Facility to define a technique for designing flight-test trajectory controllers. Many techniques have been investigated. The most promising technique of the previous research used linearizing transformations using state feedback.

In this paper we have presented a new approach to the outer-loop trajectory control problem for developing nonlinear control laws using measurement feedback. A controller was designed which applies this approach specifically to the problem of flight-test trajectory control. Testing was done on a full-envelope, nonlinear, six-degree-of-freedom simulation and in flight using an F-15 aircraft. Flight-test results are presented.

Simulation and flight-test results show that the flight-test trajectory controller can control an F-15 aircraft through level accelerations, pushover–pullups and windup turns over a large portion of the flight envelope. Some problems are encountered at high and slow (low dynamic pressure) conditions where time-scale separation between the fast and slow controllers disappears as aircraft performance decreases.

The approach combining inverse linearizing transformations with measurement feedback for designing outer-loop controllers for high performance aircraft has been validated by the results in simulation and flight testing. Since this approach does not require implicit or explicit aircraft models in the design (with the exception of a simplified engine model), it may be easily applied to other aircraft requiring similar inputs to the control system. The limitations of this approach fall into three categories

- Separation of time scales must be maintained, limiting the overall performance of the combined control and guidance system,
- nonlinearities found in the apparent linear plant must be accurately modeled so that the controller can be designed to deal with them over the entire envelope, and
- controller gains selected during analysis will probably require adjustment because of modeling inaccuracies in the analysis system, or because of nonlinearities which are not accounted for in the design of the inverse linearizing transformations.

The first limitation implies that an integrated approach can provide higher dynamic response because no time-scale separation is required. Since the time scales must be separated sufficiently for worst case plant dynamics, a penalty will be incurred when plant dynamics get faster. This may justify the use of gain scheduling for the linear controllers.

The second limitation is illustrated by the roll acceleration fed back through the stick which is described in the Implementation Experience section of this paper. While the inverse transformations as derived in this paper account for all nonlinearities in the equations of motion and the aerodynamic characteristics of the airplane, there are nonlinearities in the CAS which remain unaccounted for, and cause problems for the controller. Also, the effects of the engine nonlinearities are not completely understood at this time, however, they seem to be relatively minor.

The third limitation is common to all outer-loop design techniques. It is not unusual for control systems to be modified because of response in the simulation or in flight.

Dryden Flight Research Facility
National Aeronautics and Space Administration
Edwards, California, June 1, 1990

APPENDIX A
ILLUSTRATIVE EXAMPLE OF NONLINEAR CONTROL

To illustrate the nonlinear control method of Meyer *et al*, we present an example in which we consider a two-state model of an aircraft flying a level acceleration–deceleration

$$\dot{V} = \frac{\eta T - D}{m} - g \sin \gamma \tag{A-1}$$

$$\dot{h} = V \sin \gamma \tag{A-2}$$

In this example, V and h are the state variables; $\sin \gamma$ and η are control variables. We also assume a simple thrust and drag model defined about a trim condition represented by the subscript 0, with

$$T = T(V, h) - T_0 \tag{A-3}$$

and

$$D = D_0(V - V_0)^2 \tag{A-4}$$

For level acceleration–deceleration, we define the trajectory

$$V_{ref} = V_0 + \dot{V}_{ref} \Delta t \tag{A-5}$$

and

$$h_{ref} = h_0 \tag{A-6}$$

The nonlinear system represented by equations (A-1) and (A-2) has the form required by equation (2), with

$$\mathbf{x} = \begin{bmatrix} x_1 \\ x_2 \end{bmatrix} = \begin{bmatrix} V \\ h \end{bmatrix} \tag{A-7}$$

$$\mathbf{u} = \begin{bmatrix} u_1 \\ u_2 \end{bmatrix} = \begin{bmatrix} \eta \\ \sin \gamma \end{bmatrix} \tag{A-8}$$

$$\mathbf{f} = \begin{bmatrix} -\frac{D}{m} \\ 0 \end{bmatrix} \tag{A-9}$$

$$\mathbf{g}_1 = \begin{bmatrix} \frac{T}{m} \\ 0 \end{bmatrix} \tag{A-10}$$

$$\mathbf{g}_2 = \begin{bmatrix} -g \\ V \end{bmatrix} \tag{A-11}$$

which satisfies $\mathbf{f}[\mathbf{x}(0)] = 0$ if $\mathbf{x}(0) = \mathbf{x}_0$, the trim condition. While this is a valid representation of the nonlinear system in the form required by equation (1), it should be noted that this representation is *not* in the canonical form described by Su *et al* [32].

We consider the tracking problem by letting

$$\mathbf{y} = \begin{bmatrix} y_1 \\ y_2 \end{bmatrix} = \begin{bmatrix} V_{ref} - V \\ h_{ref} - h \end{bmatrix} \tag{A-12}$$

We will transform this system to the form shown in equation (5) by letting

$$\dot{\mathbf{y}}(t) = \mathbf{v}(t)$$

so that

$$\mathbf{v} = \begin{bmatrix} v_1 \\ v_2 \end{bmatrix} = \begin{bmatrix} \dot{V}_{ref} - \dot{V} \\ -\dot{h} \end{bmatrix} = \begin{bmatrix} \dot{V}_{ref} - \frac{\eta T - D}{m} + g \sin \gamma \\ -V \sin \gamma \end{bmatrix} \tag{A-13}$$

Assuming a linear-quadratic design, this results in pseudocontrols defined by

$$\begin{bmatrix} v_1 \\ v_2 \end{bmatrix} = \begin{bmatrix} K_{11} & K_{12} \\ K_{21} & K_{22} \end{bmatrix} \begin{bmatrix} y_1 \\ y_2 \end{bmatrix} = \begin{bmatrix} K_{11} & K_{12} \\ K_{21} & K_{22} \end{bmatrix} \begin{bmatrix} V_{ref} - V \\ h_{ref} - h \end{bmatrix} \tag{A-14}$$

From equations (A-13) and (A-14), the real controls **u** can be computed so that

$$\sin \gamma = \frac{-K_{21}(V_{ref} - V) - K_{22}(h_{ref} - h)}{V} \tag{A-15}$$

or

$$\gamma = \sin^{-1} \left[\frac{-K_{21}(V_{ref} - V) - K_{22}(h_{ref} - h)}{V} \right] \tag{A-16}$$

and

$$\eta = \frac{-m}{T} \left[K_{11}(V_{ref} - V) + K_{12}(h_{ref} - h) - g \sin \gamma - \dot{V}_{ref} \right] + \frac{D}{T} \tag{A-17}$$

which also can be expressed as

$$\eta = \frac{-m}{T} \left[\frac{(V_{ref} - V)\,[\,V K_{11} + g K_{21}\,] + (h_{ref} - h)\,[\,V K_{12} + g K_{22}\,]}{V} - \dot{V}_{ref} \right] + \frac{D}{T} \tag{A-18}$$

Three features can be observed in this simple example. The first, which is somewhat obscured by the simplifying assumptions, is that a single control law is designed to control state variables based on a reference trajectory, that is, the inner- and outer-loop control functions are combined. The second and most important feature, apparent even in this simple example is that the actual controls depend on the use of the aerodynamic and thrust models represented by D and T. Third, although the altitude and velocity command paths are clearly coupled, the control law provides decoupled control of the aircraft flightpath angle and throttle position.

APPENDIX B
DERIVATION OF NONLINEAR CONTROL LAWS FOR FLIGHT-TEST TRAJECTORY CONTROL

Nonlinear System Equations

The primary equations used to derive the WT-maps for transforming the nonlinear systems into the linear representations are given by the following equations from Duke *et al* [34]

$$\ddot{h} = a_{x,\mathrm{k}} \sin\theta - a_{y,\mathrm{k}} \sin\phi\cos\theta - a_{z,\mathrm{k}} \cos\phi\cos\theta \tag{B-1}$$

$$\dot{\alpha} = \frac{\dot{w}\cos\alpha - \dot{u}\sin\alpha}{V\cos\beta} \tag{B-2}$$

$$\dot{\phi} = p + q\sin\phi\tan\theta + r\cos\phi\tan\theta \tag{B-3}$$

$$\begin{aligned}\dot{V} &= \dot{u}\cos\alpha\cos\beta + \dot{v}\sin\beta + \dot{w}\sin\alpha\cos\beta \\ &= \frac{1}{m}[\, -D\cos\beta + Y\sin\beta + X_{\mathrm{T}}\cos\alpha\cos\beta + Z_{\mathrm{T}}\sin\alpha\cos\beta \\ &\qquad - mg(\cos\alpha\cos\beta\sin\theta - \sin\beta\sin\phi\cos\theta - \sin\alpha\cos\beta\cos\phi\cos\theta)\,]\end{aligned} \tag{B-4}$$

Additional equations used in deriving this mapping are provided by

$$\dot{h} = V(\cos\alpha\cos\beta\sin\theta - \sin\beta\sin\phi\cos\theta - \sin\alpha\cos\beta\cos\phi\cos\theta) \tag{B-5}$$

$$a_{x,\mathrm{k}} = \frac{1}{gm}(X_{\mathrm{T}} - D\cos\alpha + L\sin\alpha - gm\sin\theta) \tag{B-6}$$

$$a_{y,\mathrm{k}} = \frac{1}{gm}(Y + gm\sin\phi\cos\theta) \tag{B-7}$$

$$a_{z,\mathrm{k}} = \frac{1}{gm}(Z_{\mathrm{T}} - D\sin\alpha - L\cos\alpha + gm\cos\phi\cos\theta) \tag{B-8}$$

$$a_{x,\mathrm{k}} = a_x - \sin\theta \tag{B-9}$$

$$a_{y,\mathrm{k}} = a_y + \sin\phi\cos\theta \tag{B-10}$$

$$a_{z,\mathrm{k}} = a_z + \cos\phi\cos\theta \tag{B-11}$$

$$a_n = -a_z \tag{B-12}$$

$$M = \frac{V}{a} \tag{B-13}$$

$$\dot{u} = \frac{X_{\mathrm{T}} - gm\sin\theta - D\cos\alpha + L\sin\alpha}{m} + rV\sin\beta - qV\sin\alpha\cos\beta \tag{B-14}$$

$$\dot{v} = \frac{gm\sin\phi\cos\theta + Y}{m} + pV\sin\alpha\cos\beta - rV\cos\alpha\cos\beta \tag{B-15}$$

$$\dot{w} = \frac{Z_{\mathrm{T}} + gm\cos\phi\cos\theta - D\sin\alpha - L\cos\alpha}{m} + qV\cos\alpha\cos\beta - pV\sin\beta \tag{B-16}$$

Derivation of Pitch Control Inverse Transformation Equations

The equations related to longitudinal control, that is, the equations that ultimately result in a $\Delta n_{z_{com}}$ command to the generic high-performance aircraft model (fig. (2)), have different forms depending on the maneuver for which the

controller is intended. In this section, the derivation of the WT-map for each maneuver is presented. The derivation of the apparent linear system equations is shown for the altitude commanded control loop. The apparent linear system for each of the other command variables and control variables is similar and will not be shown explicitly.

Altitude Command

For the altitude command control loop, we use the apparent linear system defined by equation (16)

$$\dot{\tilde{\mathbf{x}}} = A\tilde{\mathbf{x}} + B\mathbf{v}$$

$$\mathbf{y} = C\tilde{\mathbf{x}}$$

with

$$\tilde{\mathbf{x}} = \begin{bmatrix} h \\ \dot{h} \end{bmatrix} \tag{B-17}$$

$$\mathbf{v} = \begin{bmatrix} v_1 \end{bmatrix} \tag{B-18}$$

$$\mathbf{y} = \begin{bmatrix} h \\ \dot{h} \end{bmatrix} \tag{B-19}$$

such that

$$\begin{bmatrix} \dot{h} \\ \ddot{h} \end{bmatrix} = \begin{bmatrix} 0 & 1 \\ 0 & 0 \end{bmatrix} \begin{bmatrix} h \\ \dot{h} \end{bmatrix} + \begin{bmatrix} 0 \\ 1 \end{bmatrix} \begin{bmatrix} v_1 \end{bmatrix} \tag{B-20}$$

and

$$\begin{bmatrix} h \\ \dot{h} \end{bmatrix} = \begin{bmatrix} 1 & 0 \\ 0 & 1 \end{bmatrix} \begin{bmatrix} h \\ \dot{h} \end{bmatrix} \tag{B-21}$$

The W-map from $\mathbf{v}$ into $\mathbf{u}$ is defined by

$$\mathbf{u} = \mathrm{W}(\mathbf{v}, \mathbf{z}) \tag{B-22}$$

For this control law, the linear system input, $\mathbf{v}$, is selected to be

$$\mathbf{v} = [\, v_1 \,] = \left[\ddot{h}_{com}\right] \tag{B-23}$$

and the nonlinear system input, $\mathbf{u}$, for the F-15 CAS is given by

$$u = \Delta n_{z_{com}} = a_{n_{com}} - 1 \tag{B-24}$$

To derive the linearizing transformation, the measurement equation for $\ddot{h}$ shown in equation (B-1) as a function of kinematic accelerations is converted to an equation for $\ddot{h}$ as a function of accelerometer outputs using equations (B-9) through (B-12) to get

$$\ddot{h} = a_x \sin\theta - a_y \sin\phi\cos\theta + a_n \cos\phi\cos\theta - 1 \tag{B-25}$$

Converting this equation from a measurement equation to a command equation with $a_n = a_{n_{com}}$ and $\ddot{h} = \ddot{h}_{com}$ gives

$$\ddot{h}_{com} = a_x \sin\theta - a_y \sin\phi\cos\theta + a_{n_{com}} \cos\phi\cos\theta - 1 \tag{B-26}$$

The linearizing transformation is obtained from this equation and equations (B-23) and (B-24) to get

$$v_1 = a_x \sin\theta - a_y \sin\phi\cos\theta + (u + 1)\cos\phi\cos\theta - 1 \tag{B-27}$$

The inverse linearizing transformation is obtained by solving the equation above for the real nonlinear input, u, so that

$$u = \frac{v_1 - a_x \sin\theta + a_y \sin\phi \cos\theta + 1}{\cos\theta \cos\phi} - 1 \tag{B-28}$$

The tracker, or pseudocontroller, for this control law will track reference altitude rate, $\dot{h}_{ref}$, and reference altitude, h_{ref}. Reference altitude rate is ramped in and out to achieve changes in altitude in the FTTC application. The resultant reference altitude input will then be parabolic which requires two integrators. A good compromise here is to use a proportional–integral–derivative (PID) controller around altitude. This will give some damping with the $\dot{h}$ term, as well as some ability to eliminate steady-state bias with the $\int h$ term, while not slowing down the control too much by having a double integral on altitude.

For this case, then, the tracking error is computed by equation (24)

$$\mathbf{e} = \mathbf{y}_{ref} - \mathbf{y}$$

with

$$\mathbf{e} = \begin{bmatrix} e_h \\ e_{\dot{h}} \end{bmatrix} \tag{B-29}$$

$$\mathbf{y}_{ref} = \begin{bmatrix} h_{ref} \\ \dot{h}_{ref} \end{bmatrix} \tag{B-30}$$

$$\mathbf{y} = \begin{bmatrix} h \\ \dot{h} \end{bmatrix} \tag{B-31}$$

so that

$$\begin{bmatrix} e_h \\ e_{\dot{h}} \end{bmatrix} = \begin{bmatrix} h_{ref} \\ \dot{h}_{ref} \end{bmatrix} - \begin{bmatrix} h \\ \dot{h} \end{bmatrix} \tag{B-32}$$

The term e_h is integrated once to get $\int e_h$ which is combined into $\mathbf{e}$ to form $\hat{\mathbf{e}}$ so that

$$\hat{\mathbf{e}} = \begin{bmatrix} \int e_h \\ e_h \\ e_{\dot{h}} \end{bmatrix} \tag{B-33}$$

The pseudocontrol can then be computed from

$$\mathbf{v} = K\hat{\mathbf{e}} = \begin{bmatrix} k_{h_I} & k_{h_P} & k_{h_D} \end{bmatrix} \begin{bmatrix} \int e_h \\ e_h \\ e_{\dot{h}} \end{bmatrix} \tag{B-34}$$

which can also be expressed as

$$v_1 = k_{h_D} e_{\dot{h}} + k_{h_P} e_h + k_{h_I} \int_{t_0}^{t_f} e_h dt \tag{B-35}$$

With these two formulations, the gain matrix K can be determined from any appropriate modern or classical control technique. Again, the designer should be careful when selecting gains so as not to make the dynamics of the pseudocontroller so fast that it can affect or be affected by the dynamics of the inner-loop control.

Normal Acceleration Command

A linear control law and inverse transformation equation are derived here for a pitch command based on normal acceleration. While it was not used for any maneuvers flown in flight test, it was implemented and tested in the simulation with good results.

For this command loop, a_n is measured directly on the aircraft so that in the nonlinear system the feedback, $\mathbf{y}$, is simply

$$\mathbf{y} = a_n \tag{B-36}$$

It is desirable to track the reference normal acceleration directly with

$$\Delta n_{z_{com}} = a_{n_{ref}} - 1$$

and

$$a_{n_{com}} = a_{n_{ref}} - a_n \tag{B-37}$$

so

$$\Delta n_{z_{com}} = a_{n_{com}} + a_n - 1 \tag{B-38}$$

Then if the pseudocontrol, v_2, is defined as

$$v_2 = a_{n_{com}} \tag{B-39}$$

and the real nonlinear control is defined as it is in equation (B-24)

$$u = \Delta n_{z_{com}}$$

The form of the linearizing transform equation would then become

$$v_2 = u - a_n + 1 \tag{B-40}$$

the inverse linearizing transformation is given by

$$u = v_2 + a_n - 1 \tag{B-41}$$

The tracking error is defined by

$$e_{a_n} = a_{n_{ref}} - a_n \tag{B-42}$$

The error is integrated once and the combined error vector is

$$\hat{\mathbf{e}} = \begin{bmatrix} \int e_{a_n} \\ e_{a_n} \end{bmatrix} \tag{B-43}$$

Since the plant dynamics are algebraic, a proportional plus integral control law is used for this control task. The pseudocontrol, then, is computed using the following equation

$$\mathbf{v} = K\hat{\mathbf{e}} = \begin{bmatrix} k_{a_{n_I}} & k_{a_{n_P}} \end{bmatrix} \begin{bmatrix} \int e_{a_n} \\ e_{a_n} \end{bmatrix} \tag{B-44}$$

Angle-of-Attack Command

The angle-of-attack command control law requires two outer-loop layers as opposed to the single layer outer-loop laws required for altitude control and normal acceleration control. The reason for this will be apparent as the linearizing transformation for the outermost layer is derived.

For the outermost loop of this control law, the pseudocontrol, v_3, is defined to be

$$v_3 = \dot{\alpha}_{com} \tag{B-45}$$

and the real nonlinear input is shown in equation (B-24)

$$u = \Delta n_{z_{com}} = a_{n_{com}} - 1$$

The linearizing transform equation is based on the observation equation for angle-of-attack rate given by equation (B-2)

$$\dot{\alpha} = \frac{\dot{w}\cos\alpha - \dot{u}\sin\alpha}{V\cos\beta}$$

The terms $\dot{w}$ and $\dot{u}$ in this equation are transformed from the force equations shown in equations (B-16) and (B-14) to kinematic acceleration equations by using equations (B-8) and (B-6) to get

$$\dot{w} = g a_{z,k} + V(q\cos\alpha\cos\beta - p\sin\beta) \tag{B-46}$$

$$\dot{u} = g a_{x,k} + V(r\sin\beta - q\sin\alpha\cos\beta) \tag{B-47}$$

These equations are transformed into functions of accelerometers by using equations (B-11), (B-12), and (B-9) to get

$$\dot{w} = -g(a_n - \cos\phi\cos\theta) + V(q\cos\alpha\cos\beta - p\sin\beta) \tag{B-48}$$

$$\dot{u} = g(a_x - \sin\theta) + V(r\sin\beta - q\sin\alpha\cos\beta) \tag{B-49}$$

Substituting $\dot{w}$ using equation (B-48) and $\dot{u}$ using equation (B-49) into equation (B-2) gives an expression for $\dot{\alpha}$ in terms of accelerometer outputs

$$\dot{\alpha} = \frac{1}{V\cos\beta}[-g(a_n\cos\alpha + a_x\sin\alpha - \cos\alpha\cos\phi\cos\theta - \sin\alpha\sin\theta)] + q - \tan\beta(p\cos\alpha + r\sin\alpha) \tag{B-50}$$

While this equation does describe $\dot{\alpha}$ as a function of a_n, taking the derivative $\frac{\partial\dot{\alpha}}{\partial a_n}$ gives

$$\frac{\partial\dot{\alpha}}{\partial a_n} = \frac{-g\cos\alpha}{V\cos\beta} \tag{B-51}$$

Unfortunately, this derivative shows the wrong sign indicating that as $\dot{\alpha}$ increases, a_n decreases. This would produce aircraft motion opposite to what is desired when commanding angle-of-attack rate.

It is required then to break up this controller into two control laws. The innermost layer of the outer-loop controller will make a pitch rate command available to the outermost layer. The outermost layer then will use a command equation similar to the $\dot{\alpha}$ equation shown in equation (B-50).

For the innermost layer of the outer-loop controller, the linear input is

$$v_{3_i} = q_{com} - q \tag{B-52}$$

and the nonlinear system input is the same as in equation (B-24)

$$u = \Delta n_{z_{com}} = a_{n_{com}} - 1$$

The pitch rate command equation is obtained by solving the $\dot{\alpha}$ equation (eq. (B-50)) for a_n. The equation is then changed into a command equation by replacing a_n with $a_{n_{com}}$ and q with q_{com}. This gives a new equation

$$a_{n_{com}} = \frac{1}{g\cos\alpha}\{V\cos\beta[\,q_{com} - \dot{\alpha} - \tan\beta(p\cos\alpha + r\sin\alpha)\,] + g(\cos\alpha\cos\phi\cos\theta + \sin\alpha\sin\theta - a_x g\sin\alpha)\} \tag{B-53}$$

Then substituting in equation (B-50) for $\dot{\alpha}$ gets

$$a_{n_{com}} = a_n + \left(\frac{V\cos\beta}{g\cos\alpha}\right)(q_{com} - q) \tag{B-54}$$

Finally, after substituting in the definitions of the linear input and the nonlinear real input, v_{3_i} and u respectively, the inverse linearizing transformation becomes

$$u = -1 + a_n + \left(\frac{V\cos\beta}{g\cos\alpha}\right)v_{3_i} \tag{B-55}$$

Since the input to the α controller is expected to be a ramp, the input into this control should also be a ramp. Therefore, only one integrator will be required, and the vectors $\mathbf{e}$ and $\hat{\mathbf{e}}$ will be

$$\mathbf{e} = [e_q] = q_{com} - q \tag{B-56}$$

and

$$\hat{\mathbf{e}} = \begin{bmatrix} \int e_q \\ e_q \end{bmatrix} \tag{B-57}$$

The pseudocontrol, v_{3_i}, can then be found from

$$v_{3_i} = \begin{bmatrix} K_{q_I} K_{q_P} \end{bmatrix}\begin{bmatrix} \int e_q \\ e_q \end{bmatrix} \tag{B-58}$$

The linearizing transform of the outermost layer of this control is found by first solving equation (B-50) for q and then replacing the q and $\dot{\alpha}$ terms with q_{com} and $\dot{\alpha}_{com}$. This gives the equation

$$q_{com} = \dot{\alpha}_{com} + \tan\beta(p\cos\alpha + r\sin\alpha) - \frac{1}{V\cos\beta}[\,-g(a_n\cos\alpha + a_x\sin\alpha - \cos\alpha\cos\phi\cos\theta - \sin\alpha\sin\theta)\,] \tag{B-59}$$

Then by defining the linear system input and the real nonlinear input as

$$v_3 = \dot{\alpha}_{com} \tag{B-60}$$

and

$$u_{3_i} = q_{com} \tag{B-61}$$

and applying these substitutions to equation (B-59) inverse linearizing transform is obtained as

$$u_{3_i} = v_3 + \tan\beta(p\cos\alpha + r\sin\alpha) - \frac{1}{V\cos\beta}[\,-g(a_n\cos\alpha + a_x\sin\alpha - \cos\alpha\cos\phi\cos\theta - \sin\alpha\sin\theta)\,] \tag{B-62}$$

It may seem disconcerting that equation (B-50) is used so often. In fact, that equation, using measurement values, is used only once in obtaining equation (B-54). In all other instances, equation (B-50) is first transformed into a command equation by replacing $\dot{\alpha}$ with $\dot{\alpha}_{com}$, or a_n with $a_{n_{com}}$, or q with q_{com}. In these circumstances, the $\dot{\alpha}$ equation is no longer a measurement equation.

The pseudocontrol law for the outer layer will contain only one integrator since the angle of attack is expected to be a ramped command. Therefore, the $\mathbf{e}$ and $\hat{\mathbf{e}}$ vectors are defined to be

$$\mathbf{e} = [e_\alpha] = \alpha_{ref} - \alpha \tag{B-63}$$

and

$$\hat{\mathbf{e}} = \begin{bmatrix} \int e_\alpha \\ e_\alpha \end{bmatrix} \tag{B-64}$$

The pseudocontrol, v_3, can then be found from

$$v_3 = \begin{bmatrix} K_{\alpha_I} K_{\alpha_P} \end{bmatrix} \begin{bmatrix} \int e_\alpha \\ e_\alpha \end{bmatrix} \tag{B-65}$$

The designer must be aware that gains need to be selected carefully for this control loop since the dynamics of the outermost layer of this control law must be slower than the innermost layer. The dynamics of the innermost layer, in turn, should be slower than the plant dynamics. Violating either of these requirements will lead to poor control of the system or even drive the system unstable.

After completing this derivation, the designer should notice that this control law provides not only a method of tracking an angle-of-attack command, but also a method of tracking a pitch rate command.

Derivation of Roll Control Inverse Transformation Equations

The equations used to provide roll control are derived here. As with the pitch commands, there are several modes depending on the reference parameter to be tracked. The real nonlinear command required by the F-15 CAS is roll rate, p_{com}. That is

$$u = p_{com} \tag{B-66}$$

Roll Attitude Command

For the roll attitude command control law, the pseudocontrol, v_4, is defined as

$$v_4 = \dot{\phi}_{com} \tag{B-67}$$

The linearizing transformation equation is derived by using equation (B-3)

$$\dot{\phi} = p + q \sin\phi \tan\theta + r \cos\phi \tan\theta$$

and substituting in $\dot{\phi}_{com} = \dot{\phi}$ and $p_{com} = p$ to get

$$\dot{\phi}_{com} = p_{com} + q \sin\phi \tan\theta + r \cos\phi \tan\theta \tag{B-68}$$

Incorporating equations (B-66) and (B-67) then gives the linearizing transform

$$v_4 = u + q \sin\phi \tan\theta + r \cos\phi \tan\theta \tag{B-69}$$

From this, the inverse linearizing transform is obtained which is

$$u = v_4 - q \sin \phi \tan \theta - r \cos \phi \tan \theta \tag{B-70}$$

The pseudocontrol is computed using a proportional-integral control law since most inputs are expected to be ramps or steps. For this control law, the **e** and $\hat{\mathbf{e}}$ vectors are

$$\mathbf{e} = [e_\phi] = \phi_{ref} - \phi \tag{B-71}$$

and

$$\hat{\mathbf{e}} = \begin{bmatrix} \int e_\phi \\ e_\phi \end{bmatrix} \tag{B-72}$$

Therefore, the equation to compute the pseudocontrol is

$$v_4 = \begin{bmatrix} K_{\phi_I} K_{\phi_P} \end{bmatrix} \begin{bmatrix} \int e_\phi \\ e_\phi \end{bmatrix} \tag{B-73}$$

The same requirements apply here as in the pitch control laws regarding the speed of the dynamics in the plant and in the outer-loop controller. The only difference is that the aircraft is very fast in the roll axis, so that the linear controller dynamics can be very fast as well.

Altitude Command

The altitude commanded roll control law is another multilayer control like the angle-of-attack commanded pitch control. The outer layer of this control law generates a roll attitude reference based on the altitude and altitude rate commands. The reference roll attitude is then used in a roll attitude command control law identical to the one shown in the previous section.

For this control law, the pseudocontrol, v_5, is defined as

$$v_5 = \ddot{h}_{com} \tag{B-74}$$

and the real nonlinear control is defined as in equation (B-66)

$$u = p_{com}$$

The intermediate real nonlinear control is defined as

$$u_{5_i} = \phi_{com} \tag{B-75}$$

The linearizing transformation used here is obtained from the vertical acceleration equation as a function of accelerometer outputs which is derived in equation (B-25) in the Derivation of Pitch Control Inverse Transformation Equations section

$$\ddot{h} = a_x \sin \theta - a_y \sin \phi \cos \theta + a_n \cos \phi \cos \theta - 1$$

This measurement equation is converted to a command equation by substituting $\phi = \phi_{com}$ and $\ddot{h} = \ddot{h}_{com}$ into it to get

$$\ddot{h}_{com} = a_x \sin \theta - a_y \sin \phi_{com} \cos \theta + a_n \cos \phi_{com} \cos \theta - 1 \tag{B-76}$$

From this and equations (B-75) and (B-74) the linearizing transformation is obtained as

$$v_5 = a_x \sin \theta - a_y \sin u_{5_i} \cos \theta + a_n \cos u_{5_i} \cos \theta - 1 \tag{B-77}$$

The inverse linearizing transformation is obtained by solving equation (B-76) for ϕ_{com} using the trigonometric identity that given

$$a\cos\phi + b\sin\phi = c \tag{B-78}$$

with

$$c^2 \leq a^2 + b^2 \tag{B-79}$$

then

$$\phi = \tan^{-1}\frac{b}{a} + \cos^{-1}\frac{c}{\sqrt{a^2 + b^2}} \tag{B-80}$$

which gives

$$\phi_{com} = +\tan^{-1}\left(\frac{a_y}{-a_n}\right) + \cos^{-1}\left(\frac{-\ddot{h}_{com} + a_x\sin\theta - 1}{\cos\theta\sqrt{{a_y}^2 + {a_n}^2}}\right) \tag{B-81}$$

Care must be taken with this equation to ensure that the angles obtained from each of the terms fall in the correct quadrants. Using this equation and substituting $v_5 = \ddot{h}_{com}$ and $u_{5_i} = \phi_{com}$ into it gives the inverse linearizing transformation

$$u_{5_i} = -\tan^{-1}\left(\frac{a_y}{-a_n}\right) - \cos^{-1}\left(\frac{-v_5 + a_x\sin\theta - 1}{\cos\theta\sqrt{{a_y}^2 + {a_n}^2}}\right) \tag{B-82}$$

The form of the pseudocontrol is identical to the form used in the pitch control of altitude shown in the Derivation of Pitch Control Inverse Transformation Equations section in equation (B-34)

$$\mathbf{v} = K\hat{\mathbf{e}} = \begin{bmatrix} k_{h_I} & k_{h_P} & k_{h_D} \end{bmatrix}\begin{bmatrix} \int e_h \\ e_h \\ \dot{e}_h \end{bmatrix} \tag{B-83}$$

At this point, the commanded roll attitude, ϕ_{com}, is selected as ϕ_{ref} and

$$v_{5_i} = \dot{\phi}_{com} \tag{B-84}$$

The inner layer control can then be determined using the roll attitude controller described in the Roll Attitude Command section.

During gain selection, the inner layer of the outer-loop control can be similar, if not the same as those in the roll attitude controller. Again, the gains for the outer layer must be selected to produce slower dynamics than the inner layer to avoid invalidating the assumption of time-scale separation.

Mach Number Command

The Mach number commanded roll control was not flight tested, however it was implemented and tested in the simulation. It is used to track Mach number with roll attitude during maneuvers with fixed throttle at load factors greater than one, such as a thrust-limited windup turn.

This control law is also a multilayer controller. In this case, however, the control law has three layers. The outermost layer generates an altitude rate command, then feeds it into an altitude commanded roll controller identical to the one discussed in the previous section which accounts for the other two layers in this controller.

For this control law, the pseudocontrol is defined to be

$$v_6 = \dot{M}_{com} \tag{B-85}$$

while the real nonlinear control is again shown in equation (B-66)

$$u = p_{com}$$

The first intermediate real nonlinear control is defined to be

$$u_{6_i} = \dot{h}_{com} \tag{B-86}$$

The linearizing transformation is derived from equations (B-4) through (B-16). First, the velocity rate terms, $\dot{u}$, $\dot{v}$, and $\dot{w}$, are converted from functions of forces to functions of kinematic accelerations by substituting in equations (B-6) through (B-8) to get

$$\dot{u} = g a_{x,k} + rV \sin\beta - qV \sin\alpha \cos\beta \tag{B-87}$$

$$\dot{v} = g a_{y,k} + pV \sin\alpha \cos\beta - rV \cos\alpha \cos\beta \tag{B-88}$$

$$\dot{w} = g a_{z,k} + qV \cos\alpha \cos\beta - pV \sin\beta \tag{B-89}$$

Then, substitutions of accelerometer outputs for kinematic accelerations are made using equations (B-9), (B-10), (B-11), and (B-12) to get

$$\dot{u} = g(a_x - \sin\theta) + rV \sin\beta - qV \sin\alpha \cos\beta \tag{B-90}$$

$$\dot{v} = g(a_y + \sin\phi \cos\theta) + pV \sin\alpha \cos\beta - rV \cos\alpha \cos\beta \tag{B-91}$$

$$\dot{w} = -g(a_n - \cos\phi \cos\theta) + qV \cos\alpha \cos\beta - pV \sin\beta \tag{B-92}$$

These equations are substituted into equation (B-4) and terms are cancelled to get

$$\dot{V} = g(a_x \cos\alpha \cos\beta + a_y \sin\beta - a_n \sin\alpha \cos\beta + \sin\phi \cos\theta \sin\beta - \sin\theta \cos\alpha \cos\beta + \cos\phi \cos\theta \sin\alpha \cos\beta) \tag{B-93}$$

Next, equation (B-5) is solved for $\frac{\dot{h}}{V}$ and is substituted into the gravity term of equation (B-93) giving

$$\dot{V} = g\left(a_x \cos\alpha \cos\beta + a_y \sin\beta - a_n \sin\alpha \cos\beta - \frac{\dot{h}}{V}\right) \tag{B-94}$$

The derivative of equation (B-13) assuming constant acoustic velocity, is taken so that

$$\dot{M} = \frac{\dot{V}}{a} \tag{B-95}$$

and incorporated into equation (B-94) to give the measurement equation for $\dot{M}$

$$\dot{M} = \frac{g}{a}\left(a_x \cos\alpha \cos\beta + a_y \sin\beta - a_n \sin\alpha \cos\beta - \frac{\dot{h}}{V}\right) \tag{B-96}$$

This measurement equation is converted to a command equation by setting $\dot{M} = \dot{M}_{com}$ and $\dot{h} = \dot{h}_{com}$ so that

$$\dot{M}_{com} = \frac{g}{a}\left(a_x \cos\alpha \cos\beta + a_y \sin\beta - a_n \sin\alpha \cos\beta - \frac{\dot{h}_{com}}{V}\right) \tag{B-97}$$

This equation is converted to the linearizing transformation by using equations (B-85) and (B-86) to get

$$v_6 = \frac{g}{a}\left(a_x \cos\alpha \cos\beta + a_y \sin\beta - a_n \sin\alpha \cos\beta - \frac{u_{6_i}}{V}\right) \tag{B-98}$$

To get the inverse linearizing transformation, this equation is solved for u_{6_i}

$$u_{6_i} = \frac{-v_6 aV}{g} + V\left(a_x \cos\alpha\cos\beta + a_y \sin\beta - a_n \sin\alpha\cos\beta\right) \tag{B-99}$$

The pseudocontrol for this layer of the controller is simply a proportional-integral controller giving the following form

$$v_4 = \begin{bmatrix} K_{M_I} K_{M_P} \end{bmatrix} \begin{bmatrix} \int e_M \\ e_M \end{bmatrix} \tag{B-100}$$

The gains selected for this linear control law must not violate the separation of time scales for the inner layers. This control is, in general, a little bit slow and has difficulty maintaining precise control of Mach number.

Derivation of Thrust Control Inverse Transformation Equations

There were three controllers developed for thrust control: a Mach number controller, a velocity controller, and a direct throttle command. The direct throttle command is trivial and is not addressed here. The velocity command is derived here, but was not tested in the simulation or in flight.

The command required onboard the aircraft is PLA

$$u = PLA_{com} \tag{B-101}$$

The inverse linearizing transforms used for this controller give an intermediate command value of thrust

$$u_i = X_{T_{com}} \tag{B-102}$$

which is converted to PLA_{com} using an inverse thrust model

$$PLA_{com} = g(X_{T_{com}}, h, M) \tag{B-103}$$

The thrust model itself is used to estimate the thrust generated by the engines at the current PLAs. The model used is a simple version of the one used in the F-15 simulation. In this model, $X_{T_{est}} = f(PLA, h, M)$. The model has three PLA break points, three Mach number break points, and two altitude break points. The model uses linear interpolation between break points, and incorporates a simple lag, $\frac{5}{s+5}$, to model engine dynamics.

Mach Number Command

For this controller, the real nonlinear control is shown in equation (B-101) and the linear control is defined as

$$v_7 = \dot{M}_{com} \tag{B-104}$$

The linearizing transform is derived from equation (B-4). To accomplish this, the equations for accelerometer outputs as functions of forces are derived by combining equations (B-6) through (B-8) with equations (B-9) through (B-12) which give

$$a_x = \frac{1}{gm}\left(X_T - D\cos\alpha + L\sin\alpha\right) \tag{B-105}$$

$$a_y = \frac{1}{gm} Y \tag{B-106}$$

$$a_n = \frac{1}{gm}\left(-Z_T + D\sin\alpha + L\cos\alpha\right) \tag{B-107}$$

Next, equation (B-105) is multiplied by $\cos\alpha$, and equation (B-107) is multiplied by $-\sin\alpha$, and the two resulting equations are added together and reordered to get

$$Z_T \sin\alpha - D = gm(a_x \cos\alpha - a_n \sin\alpha) - X_T \cos\alpha \qquad \text{(B-108)}$$

For this equation, the accelerometer variables are measured, and the X-thrust variable is estimated with the thrust model so that $X_T = X_{T_{est}}$ which gives

$$Z_T \sin\alpha - D = gm(a_x \cos\alpha - a_n \sin\alpha) - X_{T_{est}} \cos\alpha \qquad \text{(B-109)}$$

This equation is substituted into equation (B-4) to eliminate the $Z_T \sin\alpha - D$ expression and equation (B-106) is substituted in to eliminate the Y-axis force terms giving

$$\dot{V} = \frac{1}{m}\{\cos\beta[gm(a_x \cos\alpha - a_n \sin\alpha) - X_{T_{est}} \cos\alpha] + gma_y \sin\beta + X_T \cos\alpha \cos\beta +$$
$$- mg(\cos\alpha \cos\beta \sin\theta - \sin\beta \sin\phi \cos\theta - \sin\alpha \cos\beta \cos\phi \cos\theta)\} \qquad \text{(B-110)}$$

The next step is to change the equation from $\dot{V}$ to $\dot{M}$ using equation (B-95) to get

$$\dot{M} = \frac{1}{am}[\cos\beta(gm(a_x \cos\alpha - a_n \sin\alpha) - X_{T_{est}} \cos\alpha) + gma_y \sin\beta + X_T \cos\alpha \cos\beta +$$
$$- mg(\cos\alpha \cos\beta \sin\theta - \sin\beta \sin\phi \cos\theta - \sin\alpha \cos\beta \cos\phi \cos\theta)] \qquad \text{(B-111)}$$

This equation is transformed from a measurement equation to a command equation by setting $\dot{M} = \dot{M}_{com}$ and $X_T = X_{T_{com}}$ to get

$$\dot{M}_{com} = \frac{1}{am}[\cos\beta(gm(a_x \cos\alpha - a_n \sin\alpha) - X_{T_{est}} \cos\alpha) + gma_y \sin\beta + X_{T_{com}} \cos\alpha \cos\beta +$$
$$- mg(\cos\alpha \cos\beta \sin\theta - \sin\beta \sin\phi \cos\theta - \sin\alpha \cos\beta \cos\phi \cos\theta)] \qquad \text{(B-112)}$$

By using equations (B-102) and (B-104) this equation becomes the linearizing transform equation

$$v_7 = \frac{1}{am}[\cos\beta(gm(a_x \cos\alpha - a_n \sin\alpha) - X_{T_{est}} \cos\alpha) + gma_y \sin\beta + u_i \cos\alpha \cos\beta +$$
$$- mg(\cos\alpha \cos\beta \sin\theta - \sin\beta \sin\phi \cos\theta - \sin\alpha \cos\beta \cos\phi \cos\theta)] \qquad \text{(B-113)}$$

which is subsequently solved for u_i to get the inverse linearizing transform

$$u_i = \frac{1}{\cos\alpha \cos\beta}\{v_7 am - \cos\beta[gm(a_x \cos\alpha - a_n \sin\alpha) - X_{T_{est}} \cos\alpha] - gm$$
$$(a_y \sin\beta - \cos\alpha \cos\beta \sin\theta + \sin\beta \sin\phi \cos\theta + \sin\alpha \cos\beta \cos\phi \cos\theta)\} \qquad \text{(B-114)}$$

The real nonlinear control is obtained using the intermediate command value of thrust, u_i, and the inverse engine model. This can be represented mathematically by combining equations (B-101), (B-102), and (B-103) to get

$$u = g(u_i, h, M) \qquad \text{(B-115)}$$

The dynamics of the engine were not modeled in the inverse thrust model.

Since this command is expected to be either a constant or a ramp, the linear control required is a proportional-integral control law similar to the one shown in equation (B-100)

$$v_4 = \begin{bmatrix} K_{M_I} K_{M_P} \end{bmatrix} \begin{bmatrix} \int e_M \\ e_M \end{bmatrix}$$

The gains selected for this controller need to be slow enough to account for time-scale separation between the linear controller and the engine dynamics or the thrust model lag (they should be approximately the same).

Velocity Command

For velocity control of PLA, equation (B-110) is used and the linear control is defined as

$$v_8 = \dot{V}_{com} \tag{B-116}$$

The real nonlinear control remains the same as in equation (B-101)

$$u = PLA_{com}$$

and the intermediate control also remains the same

$$u_i = X_{T_{com}}$$

The linearizing transform, which is obtained from equation (B-110), would then be

$$v_8 = \frac{1}{m}[\cos\beta(gm(a_x\cos\alpha - a_n\sin\alpha) - X_{T_{est}}\cos\alpha) + gma_y\sin\beta + u_i\cos\alpha\cos\beta + \\ - mg(\cos\alpha\cos\beta\sin\theta - \sin\beta\sin\phi\cos\theta - \sin\alpha\cos\beta\cos\phi\cos\theta)] \tag{B-117}$$

and the inverse linearizing transform would be

$$u_i = \frac{1}{\cos\alpha\cos\beta}\{v_8 m - \cos\beta[gm(a_x\cos\alpha - a_n\sin\alpha) - X_{T_{est}}\cos\alpha] - gm \\ (a_y\sin\beta - \cos\alpha\cos\beta\sin\theta + \sin\beta\sin\phi\cos\theta + \sin\alpha\cos\beta\cos\phi\cos\theta)\} \tag{B-118}$$

Since the velocity command is similar to the Mach number command, the control required is a proportional integral control law similar to the one shown in equation (B-100), except in terms of velocity so that

$$v_4 = \begin{bmatrix} K_{V_I} K_{V_P} \end{bmatrix} \begin{bmatrix} \int e_V \\ e_V \end{bmatrix} \tag{B-119}$$

The same limitations on gain selection as in the Mach number command in the previous section apply to this controller.

REFERENCES

1. Burcham, Frank W., Jr., Gary A. Trippensee, David F. Fisher, and Terrill W. Putnam, *Summary of Results of NASA F-15 Flight Research Program*, NASA TM-86811, 1986.

2. Menon, P.K.A., M.E. Badgett, R.A. Walker, and E.L. Duke, "Nonlinear Flight Test Trajectory Controllers for Aircraft," *J. Guidance, Control, and Dynamics*, vol. 10, no. 1, Jan.–Feb. 1987, pp. 67–72.

3. Menon, P.K.A., M.E. Badgett, and R.A. Walker, *Nonlinear Maneuver Autopilot For The F-15 Aircraft*, NASA CR-179442, 1985.

4. Meyer, George and Luigi Cicolani, *A Formal Structure For Advanced Automatic Flight-Control Systems*, NASA TN D-7940, 1975.

5. Meyer, George and Luigi Cicolani, "Application of Nonlinear Systems Inverses to Automatic Flight Control Design — System Concepts and Flight Evaluations," AGARDograph AG-251 on *Theory and Applications of Optimal Control in Aerospace Systems*, edited by Pieter Kant, NATO, 1980, pp. 10-1 to 10-29.

6. Meyer, George, "The Design of Exact Nonlinear Model Followers," *1981 Joint Automatic Control Conference*, vol. 2, Charlottesville, VA, June 17–19, 1981, article FA-3A.

7. Meyer, G., R. Su, and L.R. Hunt, "Applications of Nonlinear Transformations to Automatic Flight Control," International Federation of Automatic Control, *Automatica*, vol. 20, no. 1, 1984, pp. 103-107.

8. Duke, Eugene L., "Automated Flight Test Maneuvers: The Development of a New Technique," 1982 Society of Flight Test Engineers (SFTE) Symposium, New York, NY, Sept. 20–22, 1982, pp. 101–119.

9. Duke, Eugene L., Michael R. Swann, Einar K. Enevoldson, and Thomas D. Wolf, "Experience with Flight Test Trajectory Guidance," *J. Guidance, Control, and Dynamics*, vol. 6, no. 5, Sept.–Oct. 1983, pp. 393–398.

10. Duke, E.L. and F.P. Jones, "Computer Control for Automated Flight Test Maneuvering," *J. Aircraft*, vol. 21, no. 10, Oct. 1984, pp. 776–782.

11. Duke, Eugene L., Frank P. Jones, and Ralph B. Roncoli, *Development and Flight Test of an Experimental Maneuver Autopilot for a Highly Maneuverable Aircraft*, NASA TP-2618, 1986.

12. Menon, P.K.A., R.A. Walker, and E.L. Duke, "Flight Test Maneuver Modeling and Control," *J. Guidance, Control, and Dynamics*, AIAA-86-0426, Jan. 1986.

13. Menon, P.K.A. and R.A. Walker, *Aircraft Flight Test Trajectory Control*, NASA CR-4161, 1988.

14. Walker, Robert and Naren Gupta, *Flight Test Trajectory Control Analysis*, NASA CR-170395, 1983.

15. Garg, Sanjay and David K. Schmidt, *Optimal Cooperative Control Synthesis of Active Displays*, NASA CR-4058, 1987.

16. Alag, Gurbux S. and Eugene L. Duke, "Development of Control Laws for a Flight Test Maneuver Autopilot," *J. Guidance, Control, and Dynamics*, vol. 9, no. 4, July–Aug. 1986, pp. 441–445.

17. Menon, P.K.A., H.A. Saberi, R.A. Walker, and E.L. Duke, "Flight Test Trajectory Controller Synthesis with Constrained Eigenstructure Assignment," 1985 4th American Control Conference, vol. 3, Boston, MA, June 19–21, 1985.

18. Antoniewicz, Robert F., Eugene L. Duke, and Brian P. Patterson, *User's Manual for Interactive LINEAR, a FORTRAN Program to Derive Linear Aircraft Models*, NASA TP-2835, 1988.

19. Duke, Eugene L., Brian P. Patterson, and Robert F. Antoniewicz, *User's Manual for LINEAR, a FORTRAN Program to Derive Linear Aircraft Models*, NASA TP-2768, 1987.

20. Smith, G.A. and George Meyer, "Total Aircraft Flight-Control System—Balanced Open- and Closed-Loop Control with Dynamic Trim Maps," IEEE Third Digital Avionics Systems Conference, Fort Worth, TX, Nov. 6–8, 1979, pp. 215-223.

21. Smith, G. Allan and George Meyer, *Application of the Concept of Dynamic Trim Control to Automatic Landing of Carrier Aircraft*, NASA TP-1512, 1980.

22. Smith, G. Allan and George Meyer, "Application of the Concept of Dynamic Trim Control and Nonlinear System Inverses to Automatic Control of a Vertical Attitude Takeoff and Landing Aircraft," AIAA-81-2238, 1981.

23. Smith, G. Allan and George Meyer, "Aircraft Automatic Digital Flight Control System With Inversion of the Model in the Feed-Forward Path," AIAA-84-2627, 1984.

24. Smith, G. Allan and George Meyer, "Aircraft Automatic Flight Control with Model Inversion," *J. Guidance, Control, and Dynamics*, vol. 10, no. 3, May–June 1987, pp. 269–275.

25. Wehrend, William R., Jr., *Pilot Control through the TAFCOS Automatic Flight Control System*, NASA TM-81152, 1979.

26. Wehrend, William R., Jr. and George Meyer, *Flight Tests of the Total Automatic Flight Control System (TAFCOS) Concept on a DHC-6 Twin Otter Aircraft*, NASA TP-1513, 1980.

27. Meyer, G., R.L. Hunt, and R. Su, *Design of a Helicopter Autopilot by Means of Linearizing Transformations*, NASA TM-84295, 1982.

28. Hunt, L.R., R. Su, and G. Meyer, "Approximating Linearizations for Nonlinear Systems," NASA TM-88772, 1986.

29. Hunt, L.R. and Renjeng Su, "Approximations of Nonlinear Systems Having Outputs," NASA CR-176946, 1984.

30. Hunt, L.R., Renjeng Su, and George Meyer, "Global Transformations of Nonlinear Systems," *IEEE Transactions on Automatic Control*, vol. AC-28, no. 1, Jan. 1983, pp. 24–31.

31. Meyer, George, Renjeng Su, and L.R. Hunt, *Applications to Aeronautics of the Theory of Transformations of Nonlinear Systems*, NASA TM-84249, 1982.

32. Su, Renjeng, L.R. Hunt, and George Meyer, *Canonical Forms for Nonlinear Systems*, NASA TM-81323, 1983.

33. Su, Renjeng and L.R. Hunt, *A Canonical Form for Nonlinear Systems*, NASA CR-176974, 1986.

34. Duke, Eugene L., Robert F. Antoniewicz, and Keith D. Krambeer, *Derivation and Definition of a Linear Aircraft Model*, NASA RP-1207, 1988.

35. Kato, Osamu and Ichiro Sugiura, "An Interpretation of Airplane General Motion and Control as Inverse Problem," *J. of Guidance, Dynamics, and Control*, vol. 9, no. 2, Mar.–Apr. 1986, pp. 198–204.

36. Cicolani, Luigi S. and Stein Weissenberger, *A Nonlinear Trajectory Command Generator for a Digital Flight-Control System*, NASA TP-1221, 1978.

REPORT DOCUMENTATION PAGE

Form Approved
OMB No. 0704-0188

1. AGENCY USE ONLY *(Leave blank)*	2. REPORT DATE	3. REPORT TYPE AND DATES COVERED
	September 1991	NASA Technical Paper

4. TITLE AND SUBTITLE

Application and Flight Test of Linearizing Transformations Using Measurement Feedback to the Nonlinear Control Problem

5. FUNDING NUMBERS

RTOP 505-60-21

6. AUTHOR(S)

Robert F. Antoniewicz, Eugene L. Duke, and P.K.A. Menon

7. PERFORMING ORGANIZATION NAME(S) AND ADDRESS(ES)

NASA Dryden Flight Research Facility
P.O. Box 273
Edwards, California 93523-0273

8. PERFORMING ORGANIZATION REPORT NUMBER

H-1629

9. SPONSORING/MONITORING AGENCY NAME(S) AND ADDRESS(ES)

National Aeronautics and Space Administration
Washington, DC 20546-0001

10. SPONSORING/MONITORING AGENCY REPORT NUMBER

NASA TP-3154

11. SUPPLEMENTARY NOTES

Robert F. Antoniewicz and Eugene L. Duke: Dryden Flight Research Facility, Edwards, California.
P. K. A. Menon: Georgia Institute of Technology, Atlanta, Georgia.

12a. DISTRIBUTION/AVAILABILITY STATEMENT

Unclassified — Unlimited
Subject Category 08

12b. DISTRIBUTION CODE

13. ABSTRACT ***(Maximum 200 words)***

The design of nonlinear controllers has relied on the use of detailed aerodynamic and engine models that must be associated with the control law in the flight system implementation. Many of these controllers have been applied to vehicle flightpath control problems and have attempted to combine both inner- and outer-loop control functions in a single controller. In this paper, a new approach to the nonlinear trajectory control problem is presented. This approach uses linearizing transformations with measurement feedback to eliminate the need for detailed aircraft models in outer-loop control applications. By applying this approach and separating the inner-loop and outer-loop functions two things are achieved: (1) the need for incorporating detailed aerodynamic models in the controller is obviated and (2) the controller is more easily incorporated into existing aircraft flight-control systems. This paper also discusses an implementation of the controller described here. This controller is tested on a six degree-of-freedom F-15 simulation and in flight on an F-15 aircraft. Simulation data are presented which validates this approach over a large portion of the F-15 flight envelope. Proof of this concept is provided by flight-test data that closely matches simulation results. Flight-test data are also presented.

14. SUBJECT TERMS

Aircraft control; Dynamic conversions; Linearizing transformations; Nonlinear control

15. NUMBER OF PAGES

56

16. PRICE CODE

A04

17. SECURITY CLASSIFICATION OF REPORT	18. SECURITY CLASSIFICATION OF THIS PAGE	19. SECURITY CLASSIFICATION OF ABSTRACT	20. LIMITATION OF ABSTRACT
Unclassified	Unclassified	Unclassified	

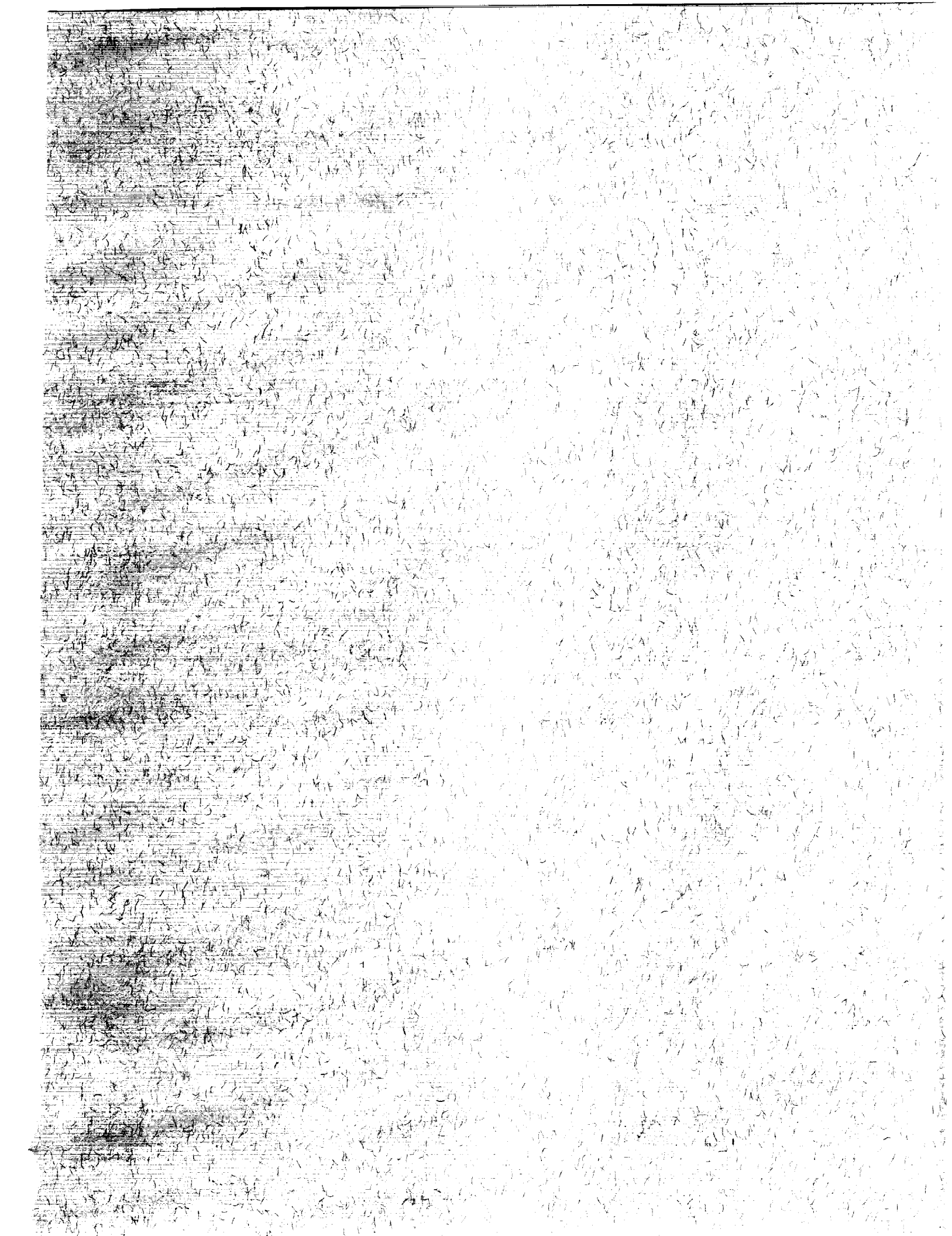

National Aeronautics and
Space Administration
Code NTT-4

Washington, D.C.
20546-0001